NEUROSCIENCE

Increased palmitoylation improves estrogen receptor alpha–dependent hippocampal synaptic deficits in a mouse model of synucleinopathy

Tim E. Moors[1], Shaomin Li[1], Thomas D. McCaffery[1], Gary P. H. Ho[1], Pascal A. Bechade[1], Luu N. Pham[2], Maria Ericsson[3], Silke Nuber[1]*

Parkinson's disease (PD) is characterized by conversion of soluble α-synuclein (αS) into intraneuronal aggregates and degeneration of neurons and neuronal processes. Indications that women with early-stage PD display milder neurodegenerative features suggest that female sex partially protects against αS pathology. We previously reported that female sex and estradiol improved αS homeostasis and PD-like phenotypes in E46K-amplified (3K) αS mice. Here, we aimed to further dissect mechanisms that drive this sex dimorphism early in disease. We observed that synaptic abnormalities were delayed in females and improved by estradiol, mediated by local estrogen receptor alpha (ERα). Aberrant ERα distribution in 3K compared to wild-type mice was paired with its decreased palmitoylation. Treatment with ML348, a de-palmitoylation inhibitor, increased ERα availability and soluble αS homeostasis, ameliorating synaptic plasticity and cognitive and motor phenotypes. Our finding that sex differences in early-disease αS–induced synaptic impairment in 3KL mice are in part mediated by palmitoylated ERα may have functional and pathogenic implications for clinical PD.

INTRODUCTION

Parkinson's disease (PD) incidence is higher in men than in women (~1.5- to 2-fold), while emerging evidence suggested that women present with a milder manifestation of certain clinical symptoms early in PD, including cognitive and motor dysfunction (*1*, *2*). In support of a partial protection in PD by female sex, women with de novo PD display increased neuronal connectivity (*3*) and lesser atrophy of hippocampal and cortical regions (*1*, *4*) compared to men. In addition, preserved striatal dopamine transporter (DAT) binding (*5*, *6*) may partially underlie enhanced responses to levodopa in women with PD (*7*, *8*). Although male sex is a well-known risk factor for PD, the mechanisms that contribute to protected neuronal function in female PD brains remain challenging because of the complexity of studying highly multifaceted sexual dimorphisms in the aging human brain. Previous studies suggested that factors reducing estrogen exposure during life were associated with higher risk of developing PD (*5*, *9*–*11*). In support of a protective role of estrogen in PD, case-control studies have shown that estrogen replacement therapy mitigates PD symptoms (*12*, *13*) and decreases PD risk (*14*) in women. Although efficacy of estrogen therapy in PD has been debated in light of detrimental side effects such as stroke and breast cancer (*15*), a better understanding of cellular pathways underlying estrogen-based female resilience to specific pathological events could provide important insights into protective pathways that may be stimulated in therapies for PD.

A central player in the pathophysiology of PD [and related synucleinopathies such as dementia with Lewy bodies (DLB)] is α-synuclein (αS), an abundant soluble protein in the brain, which, in disease, turns insoluble for currently unknown reasons and accumulates into neuronal inclusions termed Lewy bodies (LBs) and Lewy neurites (*16*). Under physiological conditions, αS is mainly enriched in presynaptic terminals, where it transiently interacts with synaptic vesicles (SVs), regulating their clustering, trafficking, and exocytosis (*17*–*19*). Increasing evidence suggests that the dynamic conversion of αS monomers (14 kDa) into soluble and helical multimers (e.g., 60-/80-/100-kDa species) plays a role in αS homeostasis and its physiological functions (*18*–*21*). In accordance with the synaptic localization and functions of αS, it is widely believed that early αS accumulation in PD starts at presynaptic sites, followed by its pathological redistribution to and engagement of other subcellular locations (*22*–*24*). LBs were shown to be enriched in lipids and vesicular structures in nigral and hippocampal neurons (*25*) and abundant in SV-related proteins (*26*), suggesting coaggregation of αS with SV membranes. Patients with PD dementia and DLB exhibit substantial cortical and hippocampal LB pathology (*27*, *28*) and high levels of insoluble αS in the hippocampus (*29*), suggesting that αS pathology in these regions is an important pathological correlate for cognitive symptoms such as dementia.

To promote the pathological interaction between αS monomers and membrane lipids, we amplified the familial PD-causing E46K αS mutation (*30*) in the canonical repeat motifs, creating "3K" αS. We previously showed that 3K αS displays excessive membrane association, leading to lipid-rich inclusions in culture (*31*, *32*) and mice (*33*). In mice, expression of 3K αS caused an levodopa–responsive motor syndrome reminiscent of PD, manifesting as early as at 3 months of age (*33*). While 3K mice collectively showed aggravated phenotypes compared to human (hu-) E46K or wild-type (WT)–overexpressing mice (*33*), intriguingly, 3K females showed milder motor phenotypes compared to males (*34*). In the brain, this was associated with less extensive synucleinopathy and higher neurite fiber densities in females compared to males despite similar 3K

[1]Ann Romney Center for Neurologic Diseases, Brigham and Women's Hospital and Harvard Medical School, Boston, MA 02115, USA. [2]Laboratory for Drug Discovery in Neurodegeneration, Department of Neurology, Brigham and Women's Hospital and Harvard Medical School, Boston, MA 02115, USA. [3]Electron Microscopy Laboratory, Department of Cell Biology, Harvard Medical School, Boston, MA 02115, USA.
*Corresponding author. Email: snuber@bwh.harvard.edu

αS expression profiles (*34*). This suggests that female sex partially protects against modeled pathologies resulting in excessive αS monomers and lipid interactions in 3K mice. In support of a protective role of estrogen, increased brain estradiol (E2) after treating 3K mice with the prodrug 10β,17β-dihydroxyestra-1,4-dien-3-one (DHED) (*35*) increased αS solubility and multimerization, reduced aggregates, and improved motor function. These results supported previous observations of E2 neuroprotection in (1-methyl-4-phenyl-1,2,3,6-tetrahydropyridine/6-hydroxydopamine) neurotoxin-based rodent PD models (*36*–*38*). Furthermore, DHED treatment resulted in preserved dopaminergic fibers (*34*), in line with protective effects of E2 on synaptic integrity (*39*).

Since early αS pathology is thought to occur at synaptic termini, which are relatively spared in female patients with de novo PD (*5*, *6*), we hypothesized that increased estrogen levels in women may offer protection against synaptic αS–induced pathologies at early-stage disease. We here investigate the impact of sex and estrogen on synaptic function in lower-expressing 3KL mice, which have a moderate overexpression (~1-fold) of hu-3K αS (*33*, *40*). Our findings show delayed onset of motor phenotypes in 3KL female mice at 6 months, reproducing our results in higher-expressing 3K mice (*34*). We also found sparing of cognitive function in 6-month-old 3KL females, which was paired with increased αS solubility and multimerization in the hippocampus and cortex, and preserved hippocampal synaptic strength at this time point. Elevating estrogen exposure by acute E2 administration on hippocampal tissue sections and after DHED treatment improved sex-specific synaptic deficits in 3KL males at 6 months, supporting the idea that local E2-dependent pathways can compensate against the pathological insult by 3K αS. We observed that effects of DHED were blocked by selective antagonists of estrogen receptor alpha (ERα), for which immunoreactivity colocalized with αS aggregates in 3KL mice (and also in LBs in human PD/DLB brains). Since we found indications that the decreased extrasomatic ERα distribution was accompanied by its reduced palmitoylation, we investigated whether increasing palmitoylation by oral application of ML348, a small-molecule inhibitor of acylpalmitoyl-thioesterase 1 (APT1), benefits motor and cognitive phenotypes of symptomatic male and female 3KL mice. A 90-day treatment ameliorated soluble αS homeostasis, synaptic plasticity, and motor and cognitive deficits in 3KL mice. No treatment effects were observed in WT mice without overt phenotypes. Collectively, these findings support a role for extranuclear ERα in estrogen-dependent preservation of αS-induced hippocampal synaptic deficits, while our results add to recent findings suggesting therapeutic potential of targeting protein palmitoylation in PD and other neurodegenerative diseases (*41*, *42*).

RESULTS

Female sex partially preserves αS solubility and multimerization in 3KL mice

To enable the study of sexual dimorphisms in early-stage synaptic pathologies by 3K αS, we used 3KL αS mice, expressing mutant αS close to the level of mouse endogenous αS [fig. S1, A and B; see also (*33*)] because this model shows a slower and more gradual development of symptoms. Since 3KL mice showed onset of motor symptoms only at 6 to 8 months (*33*), which were not detected in juvenile mice at 2 months (fig. S2A), we decided to focus on the 6-month time point for studying early αS-induced pathologies.

We previously described the cell-penetrant cross-linker disuccinimidyl glutarate (DSG) to trap cell lysis–sensitive αS multimers in culture (*31*, *32*) and in mice (*33*, *34*). Similar to our previous in vivo studies (*33*, *34*), expression of 3K αS decreased soluble αS (60 + 80 + 100 kDa) multimers relative to (14 kDa) monomers at 6 months compared to WT αS in cortical tissue pieces [two-way analysis of variance (ANOVA), effect genotype $P < 0.0001$]. This decreased multimer:monomer ratio was more prominent in 3KL males compared to females ($P = 0.009$; Fig. 1A, more detailed statistics provided in table S1), but not accompanied by between-group differences in DJ-1, which was included as control for equal cross-linking, or actin (loading control; Fig. 1A and table S1).

We hence studied the solubility of αS monomers in sequential extractions of the hippocampus and cortex in non–cross-linked tissue after lysis by its biochemical distribution in subsequent tris-buffered saline (TBS)–soluble and –insoluble [radioimmunoprecipitation assay (RIPA)/urea-soluble] fractions (Fig. 1B). We focused on hippocampus and cortex as we observed the strongest immunoreactivity of hu-αS in these regions (Fig. 1C), consistent with the neuronal distribution of the Thy1.2 promoter. Results revealed that solubility of hu-αS was markedly decreased in 3KL versus WT mice in the hippocampus (~5-fold; two-way ANOVA, effect genotype $P < 0.0001$; Fig. 1B and table S1) and frontal cortex (fig. S1C). Results based on Western blotting (WB) quantifications were corroborated by quantitative enzyme-linked immunosorbent assays (ELISAs), with 3KL females showing a trend toward increased solubility compared to males (Fig. 1C and table S1). Results by both techniques showed increased solubility (~2-fold) in females compared to males, suggesting that female sex reduces the excessive membrane binding of 3K αS.

Furthermore, buffer-insoluble urea extracts of the hippocampus of 3KL mice revealed a higher–molecular weight (HMW) αS smear, which was more prominent in males than in females (fig. S1E), consistent with lesser accumulation of insoluble αS in females at 6 months old. In correspondence, relative protein levels (fig. S1D; $P = 0.01$) and immunohistochemical (IHC) staining (Fig. 1D and table S1; 3KL males versus females, $P = 0.007$) for pSer129 αS, a commonly used marker for LB pathology, were lower in both the hippocampus and cortex of female compared to male 3KL mice (although still increased compared to WT mice). We did not detect sex differences and only very limited pSer129 αS immunoreactivity in WT control mice (Fig. 1D).

Morphologically, pSer129 αS IHC in 3KL mice manifested as inclusions in neuronal somata and neuritic processes, while prominent synaptic-like punctate staining was additionally observed, most notably in the hippocampus (Fig. 1D). Super-resolution stimulated emission depletion (STED) microscopy further suggested that these profiles colocalized with the SV marker synapsin but to a lesser extent to the plasma membrane (PM)–associated SNAP-25, suggesting accumulation of pSer129 αS at SV in 3KL mice (Fig. 1E). To further study the synaptic association of 3K αS with SVs, we applied an antibody against hu-αS (15G7) in immuno-electron microscopy and found extensive accumulation of αS-immunogold associated with SV clusters in 6-month-old 3KL males (Fig. 1F) while significantly less αS-immunogold decorated SVs in 3KL females and WT mice at this time point ($P < 0.0001$; Fig. 1F and table S1). Overall, our findings suggest that female sex partially preserved soluble αS homeostasis in the hippocampus and cortex of 3KL mice

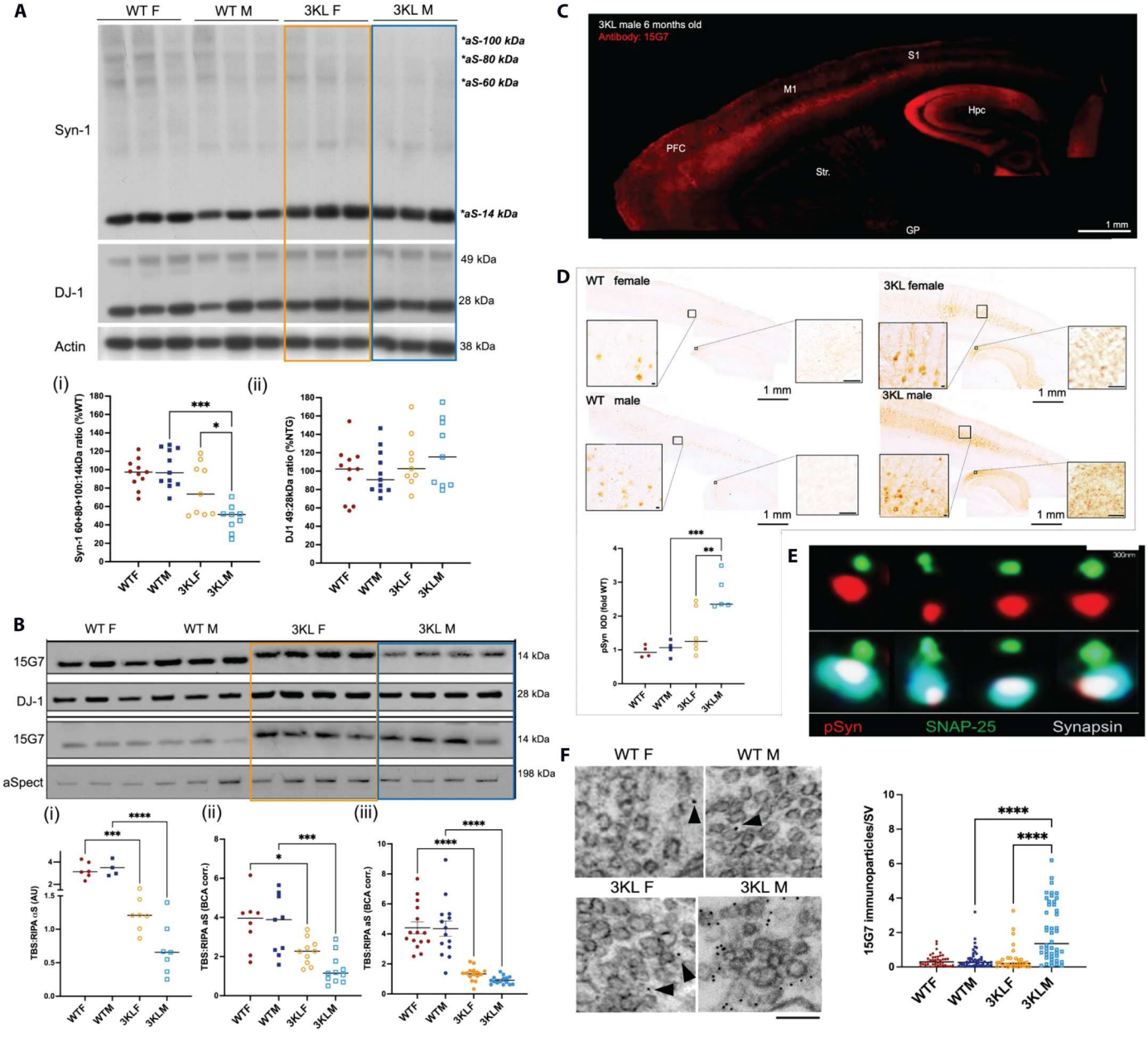

Fig. 1. Female sex partially protects against αS dyshomeostasis and pathology in hippocampus and cortex of 6-month-old 3KL mice. (**A**) Representative WB of αS (Syn-1) and DJ-1 (cross-linking control) in DSG–cross-linked 3KL/WT frontal cortex samples. Graphs: (i) Quantifications of αS multimer/monomer ratios and (ii) DJ-1 dimer/monomer ratios. (**B**) Representative WBs of hu-αS in TBS- and RIPA-soluble sequential extracts. Quantification of TBS:RIPA ratios in the hippocampus by WB (i) and ELISA (ii), and in the frontal cortex by ELISA (iii). (**C**) Expression of hu-αS over different brain regions of a Thy1.2-3KL male. (**D**) Representative images of pSer129 αS IHC in hippocampus and cortex, and quantification of integrated optical densities (IODs; $N = 4$ to 6 mice per group). Insets (left) somatic/neuritic pSer129 αS inclusions in the cortex; (right) hippocampal punctate pSer129 αS^{+} synaptic-like profiles. (**E**) Colocalization of pSer129 αS with SV-marker synapsin but not SNAP-25 in the hippocampus of a 3KL male. Deconvoluted STED images. (**F**) SV-associated hu-αS (15G7) immunogold in the hippocampus of male/female 3KL/WT (quantification of individual synapses captured in $n = 4$ sections in two mice per group). Scale bars, 1 mm [(C) and (D)]; 20 μm [(D), insets]; 300 nm (E); and 100 nm (F). (A), (C), and (D) Dot plots show data from individual mice (and median); (F) dot plots show data from individual analyzed EM micrographs in two mice per group (and median). Statistics by two-way ANOVAs [(A), (C), and (D)] or nonparametric Kruskal-Wallis test (F) and post hoc with Bonferroni/Dunn correction, respectively (see table S1); $^{*}P < 0.05$; $^{**}P < 0.01$; $^{***}P < 0.001$; $^{****}P < 0.0001$. AU, arbitrary units; aSpect, α-spectrin.

at 6 months, resulting in decreased αS accumulation at SVs and in pSer129 αS^+ inclusions.

Female sex delays the onset of motor and cognitive phenotypes and hippocampal synaptic impairment in 3KL mice

To study whether milder biochemical/histological alterations in 3KL females at 6 months associated with a beneficial phenotypic outcome, WT and 3KL male/female mice were examined in various behavioral tests paradigms—rotarod, novel-object recognition (NOR) test, and Morris water maze (MWM)—at this time point. To allow further insight into the progression of phenotypes over time, selected tests were also performed at 12 months of age.

Rotarod tests were done to assess fine motor and balancing skills of 3KL mice, which were previously shown to become impaired, resultant of progressive 3K αS pathology, with symptoms starting around 6 to 8 months in 3KL males (*33*). In line with these previous results, three-way ANOVA showed an overall significantly impaired rotarod performance ($P = 0.003$, details in table S2) in 3KL versus WT mice, based on measurements at 6 and 12 months (Fig. 2A). First symptoms in 3KL males were apparent at 6 months by reduced endurance on the rotarod compared to other groups (Fig. 2A). At this time point, 3KL males performed significantly worse than 3KL females ($P = 0.0001$). However, the performance of 3KL females dropped significantly between 6 and 12 months ($P = 0.02$) toward levels more similar to 3KL males (Fig. 2A), in line with later onset of symptoms. No significant behavioral impairments or sex-related changes were observed in the rotarod performance of age-matched WT controls at the analyzed time points (table S2), in line with our previous studies (*34*).

Given the prominent expression of 3K αS in hippocampus and cortex, and cognitive impairment being a cardinal feature of clinical PD, we additionally tested 3KL and WT male/female mice in NOR (Fig. 2B) and MWM (Fig. 2C) paradigms to test their cognitive functions. On the basis of longitudinal measurements at 6 and 12 months, we found an overall significantly decreased NOR performance of 3KL versus WT (three-way ANOVA, genotype effect: $P < 0.0001$; details in table S2). At 6 months, NOR test revealed significantly worse discrimination ratios in 3KL males compared to WT ($P = 0.006$), while 3KL females performed similar to WT and significantly better than 3KL males ($P = 0.006$; Fig. 2B). However, similar to the rotarod performance, NOR discrimination ratios of 3KL females dropped significantly between 6 and 12 months ($P = 0.001$). To rule out that these deficits were due to a lack of ambulatory activity, we measured the distance traveled in the NOR test (fig. S2B), which was not different between groups. No significant changes were observed in/between WT males/females at the different analyzed time points (table S2).

To validate the NOR results with a stringent test for long-term memory (LTM), 6-month-old 3KL and WT mice were additionally trained in an MWM and assessed after a 7-day retention period. The spatial memory was worse in 3KL males compared to females ($P = 0.004$), which performed more similar to WT (Fig. 2C and table S2). This effect was not associated with impaired learning ability (fig. S2C) or reduced velocity (fig. S2D) in the MWM test. Since we already found indications for impaired motor performance (Fig. 2A) and impaired spatial memory in the NOR (Fig. 2B) for both 3KL males and females, we did not perform an additional MWM at 12 months given attrition of repetitive testing (*43*). Together, the results in NOR and MWM are in line with delayed onset of cognitive phenotypes in 3KL females compared to males. No phenotypic changes were detected between WT females and males (table S2).

Because of indications for synaptic αS^+ accumulations in the hippocampus of 3KL mice (Fig. 1, D to F) and the associated impairment of hippocampus-dependent cognitive functions (Fig. 2, B and C), we hence conducted long-term potentiation (LTP) measurements in the hippocampal CA1 of WT and 3KL mice at 6 and 12 months. At 6 months, 3KL females showed field excitatory postsynaptic potential (fEPSP) slopes similar to WT mice (Fig. 2D). In contrast, the male 3KL Schaffer-collateral projections elicited normal initial potentiation, but this failed to stabilize, with responses decaying below WT level. Quantitative analysis of mean fEPSP slope between 55 and 60 min of LTP recording showed a significant ~24% decrease in 3KL males versus females (Fig. 2E and table S2: analysis by two-way ANOVA; post hoc 3KL males versus females: $P = 0.005$). In line with results of behavioral tests, LTP levels from 12-month 3KL female mice decreased significantly compared to 6 months (Fig. 2, D and E, and table S2; $P = 0.0004$) toward similar LTP levels as 3KL males. Together, these results suggest that hippocampal synaptic function by αS dyshomeostasis is delayed by female sex but that males and females show similar phenotypes at 12 months.

Estradiol-dependent protection of 3K αS-associated hippocampal synaptic deficits is mediated by ERα

We previously reported that elevating brain E2 by the selective prodrug DHED enhanced αS solubility and physiological multimerization and benefited motor phenotypes in 3K mice (*34*, *35*). As we found preserved synaptic function in 3KL female compared to male mice at 6 months, we hypothesized that this neuroprotection could be in part related to differences in hippocampal E2 levels between males and females. To further establish the link between sex differences in 3KL mice and E2, we investigated whether increasing E2 levels could alleviate early αS-induced synaptic impairment in 6-month-old 3KL male mice by acute E2 treatment of hippocampal tissue slices. Our results showed that acute E2 treatment increased hippocampal %fEPSP in male 3KL to physiological levels (Fig. 2, F and G). To corroborate this result, we chronically administered DHED for 21 days to WT and 3KL males and assessed synaptic function by LTP measurements. We found that after DHED treatment, fEPSP slopes in 3KL males were at similar levels as WT (Fig. 2, H and I), while WT LTP levels did not significantly change after DHED treatment. This is in line with results of previous studies that have collectively revealed a complex relationship between estrogen and synaptic function and behavior, in which intermediate doses are showing optimal effects (*44*). Our interpretation of better cognitive function and hippocampal LTP in 3KL male mice, but not WT (Fig. 2), after DHED treatment is that increased E2 exposure can compensate for specific pathological insults by 3K αS.

Since E2 is known to exert its cellular actions via binding to ERs (*45*), we studied the effects of ICI 182,780—an established ER antagonist—on increased LTP after DHED treatment in 3KL mice. We observed that ICI application of acute hippocampal slides from DHED-treated 3KL mice abolished the %fEPSP increase by DHED ($P = 0.02$; Fig. 2, H and I). To establish individual contributions of ERα and ERβ, we hence applied selective antagonists

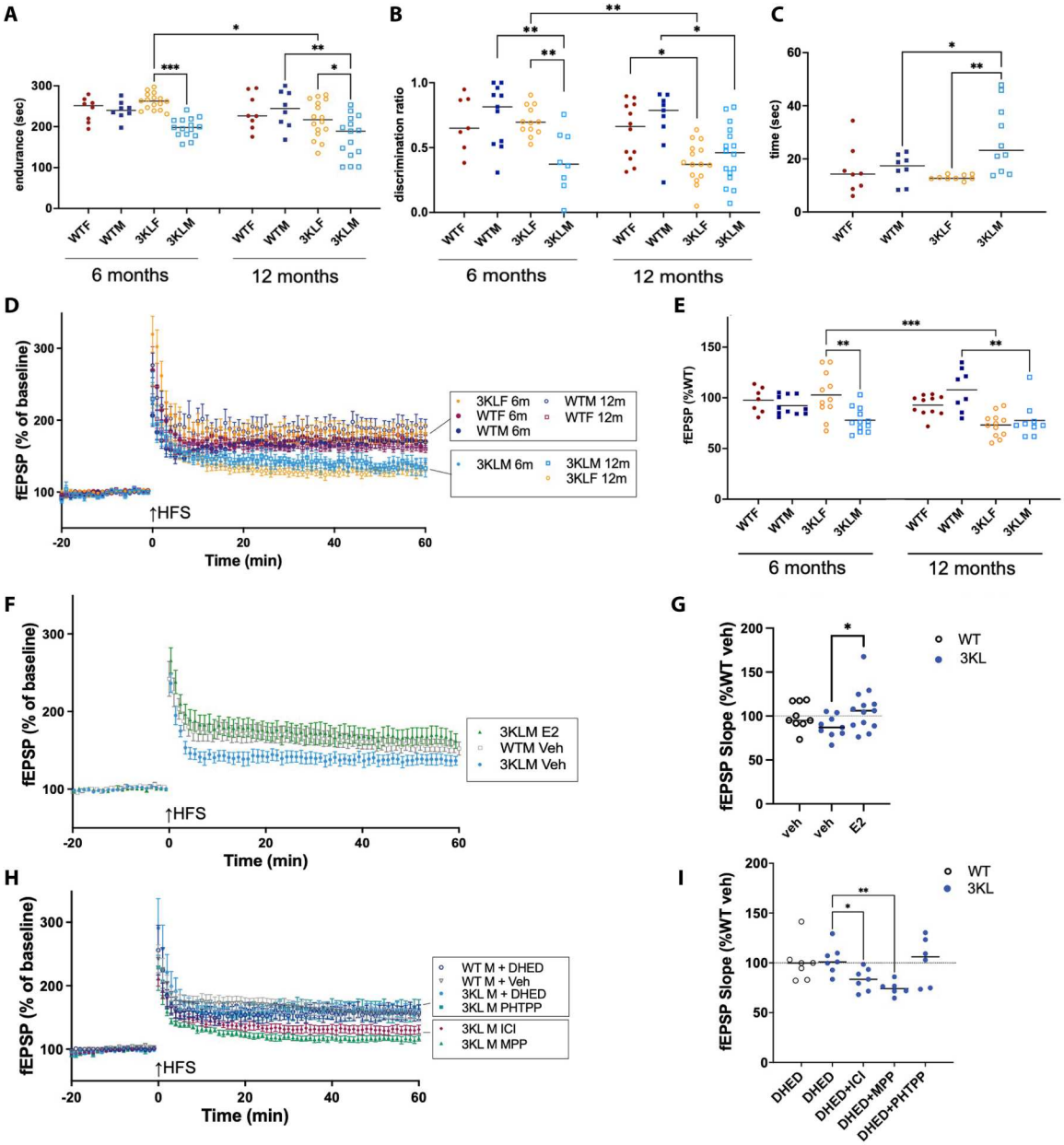

Fig. 2. Sex differences of cognitive and motor deficits associated with ERα-mediated hippocampal synaptic dysfunction in 6-month-old 3KL mice. (**A**) Assessment of fine motor and balancing skills in a rotarod test. (**B**) Discrimination ratio in the NOR test and (**C**) time to find the hidden platform in the MWM long-term spatial memory test. (**D**) Electrophysiological measurement of hippocampal LTP in acute sections of male/female 3KL versus WT mice. Mean ± SD %fEPSP slope per group are displayed over time. (**E**) Quantitation of average %fEPSP slopes during the last 5 min of measurement. (**F**) Effect of E2 application on LTP in hippocampal sections of male 3KL and WT and quantification over the last 5 min of measurement (**G**). (**H**) Selective antagonist against ERα (MPP, 1 μM) but not ERβ (PHTPP, 1 μM) reduces hippocampal LTP potentiated by DHED treatment in male 3KL. Quantification over the last 5 min of measurement in (**I**). Dot plots show data from individual mice (and median). Statistics by one-way [(G) and (I)], two-way (C), or three-way [(A), (B), and (E)] ANOVAs. (G) and (I) Statistics by targeted Student's *t* tests. **P* < 0.05; ***P* < 0.01; ****P* < 0.001. Results of planned post hoc comparisons with Bonferroni correction are presented (see table S3). HFS, high frequency stimulation.

against ERα [methyl-piperidino-pyrazole (MPP)] and ERβ (PHTPP) in acute sections of DHED-treated mice. Our measurements showed that MPP blocked the effect of DHED treatment on LTP in 3KL males (Fig. 2, H and I: −28%; one-way ANOVA; $F_{3,27} = 4.556$; $P = 0.01$; post hoc DHED versus DHED + MPP: $P = 0.02$). In contrast, PHTPP did not abolish this LTP restoration by DHED (Fig. 2, H and I; $P > 0.99$). Together, this suggests that the protective effect of E2 on hippocampal synaptic function in 3KL mice is predominantly mediated by ERα.

Aberrant ERα distribution patterns in 3KL are associated with its decreased palmitoylation

Given our finding that improvement in hippocampal synaptic strength by E2 in 3KL males is likely driven by locally available

(synaptic) ERα, we studied whether synaptic ERα distribution differs between 3KL males and females at 6 months. IHC using different selected antibodies against ERα (TE111.5D11/D8H8/SP1) in the hippocampus of WT mice displayed the expected nuclear immunoreactivity (fig. S3A). In addition, we observed punctate extrasomatic profiles for ERα in the neuropil of the hippocampal stratum oriens (SO; fig. S3, A and B), suggesting localization of ERα to neuronal processes and synapses, similar to previous descriptions of ERα immunoreactivity patterns (*46*). These findings were corroborated using immuno–transmission electron microscopy (TEM), by which we observed ERα immunogold in nucleus/nuclear envelop, dendrites and presynaptic termini (including ERα associated with SVs), and postsynaptic spines (fig. S3E).

We quantified the density of these extrasomatic ERα$^+$ profiles in different fields of the hippocampal SO in sections of 6-month-old WT/3KL males and females, scanned using high-resolution confocal microscopy. Our analyses revealed moderately reduced ERα$^+$ densities in 3KL males versus females ($P = 0.02$), while levels in 3KL females were similar to WT (Fig. 3A). We found similar results using different antibodies against ERα (e.g., D8H8 and TE111.5D11; fig. S3, B to D). Albeit reduced, 3KL still showed residual extrasomatic ERα, suggesting that local ERα–mediated protective E2 pathways are—at least in part—functional, in line with increased LTP by DHED treatment (Fig. 2, H and I). The decrease of ERα punctae was not paralleled by differences in density for the SV membrane-protein synaptophysin (Fig. 3A and table S3). While we found lower overall ERα densities in 3KL males, occasional larger ERα foci colocalizing with 15G7 in 3KL (both male and female) mice versus WT were further observed (Fig. 3B, $P < 0.0001$; table S3, more detailed images by STED in fig. S3F). These observations suggested that part of ERα may be sequestrated into synaptic 3K αS$^+$ deposits. Using an antibody against ERβ, sporadically observed extrasomatic profiles showed only limited colocalization to αS$^+$ or ERα$^+$ (fig. S3G).

The extrasomatic distribution of ERα depends on its association with the PM, which is directed by ERα palmitoylation and association with caveolin-1 (Cav1) (*47*, *48*). Therefore, we next studied the association of ERα with Cav1 using immunostainings and proximity ligation assays (PLAs). Double labeling depicted ERα puncta colocalizing with Cav1 at the cytoplasmic periphery in WT mice (fig. S3H). Upon this, we next developed an ERα:Cav1 PLA using the same antibodies. As expected, PLA signal was localized at the cytoplasmic periphery (indicated by MAP2$^+$), while barely any nuclear signal was observed, in line with the ERα:Cav1 interaction at the PM (fig. S3, I and J). Quantification of ERα:Cav1 PLA$^+$ in the hippocampal SO showed decreased signal in 3KL versus WT but being relatively spared in 3KL females (Fig. 3C, two-way ANOVA effect genotype: $P < 0.0001$; post hoc 3KL versus WT males: $P = 0.001$; post hoc 3KL versus WT females: $P = 0.007$; more details in table S3).

In addition, when studying distribution patterns of ERα, we found indications for perinuclear enrichment of ERα in 3KL mice, colocalizing with hu-αS$^+$ inclusions (Fig. 3D). Immuno-TEM corroborated this finding by perinuclear ERα immunogold in the vicinity of lipid-rich aggregates typical of 3K αS pathology (fig. S3K) (*33*, *34*). ERβ antibodies showed limited localization to perinuclear αS$^+$ inclusions and mainly revealed immunoreactivity in the nucleus regardless of the presence of αS$^+$ inclusions in 3KL/WT (fig. S3L). To determine whether ERα also localized to LBs in the PD or DLB brain, double IF experiments were conducted in postmortem tissue of patients with PD and DLB. Different antibodies against ERα, but not negative primary antibody controls (fig. S3M), demonstrated immunoreactivity in pSer129 αS$^+$ LBs of the substantia nigra (SN) and hippocampus/transentorhinal cortex (Fig. 3E). In contrast, no immunoreactivity was detected in LBs when using an antibody against ERβ (fig. S3N). To validate the impact of αS inclusion pathology on ERα nuclear versus cytoplasmic distribution, we quantified ERα$^+$ foci in nucleus and cytoplasm between cortical neurons with/without αS$^+$ inclusions and found that neurons with αS$^+$ inclusions showed fewer nuclear and more cytoplasmic ERα$^+$ than those without pathological inclusions (fig. S3O).

Together, these data suggest (early) αS dyshomeostasis by 3K decreased synaptic ERα availability, possibly affecting its transport by sequestration into perinuclear aggregates in 3KL (and also in PD/DLB tissue; summarized in Fig. 3F). At 6 months, reduced extrasomatic ERα distribution was more pronounced in 3KL males than in females, supporting a possible role for extranuclear ERα in partially protecting hippocampal synaptic function under conditions of synucleinopathy in 3KL females. As ERα palmitoylation is essential for its extranuclear distribution (*48*), we conducted acyl-biotin exchange (ABE) assays on whole-brain lysates of WT/3KL males and females in combination of downstream detection of ERα by WB. In these WBs (antibody: D8H8), the ~65-kDa form of ERα, corresponding to full-length monomeric ERα, was the major observed proteoform. While additional weaker smaller-sized (45 kDa) signals were observed in input samples, these were below detection level in ABE-processed (palmitoylated) extracts (fig. S3P). While our assays showed unambiguous signals for ~65-kDa ERα in WT mice, levels for palm-ERα were diminished in 3KL mice (Fig. 3G). Quantifications confirmed a marked reduction of ERα palmitoylation both in male and in female 3KL compared to WT (Fig. 3G; effect genotype in two-way ANOVA: $P = 0.0008$; table S3).

Inhibiting de-palmitoylation by a brain-penetrant APT1 inhibitor improves cognitive test performance and synaptic deficits in 3KL mice

Since we found that ERα palmitoylation was decreased in male and female 3KL (Fig. 3G), developing estrogen-dependent synaptic deficits between ages 6 and 12 months (Fig. 2), we hypothesized that increasing local ERα palmitoylation could potentiate protective responses and alleviate the observed phenotypes. Previous studies reported that APT inhibitors (such as palmostatin B) reduced depalmitoylation of ERα, thereby prolonging its membrane availability (*49*) and making it less vulnerable for degradation (*50*). In addition, the in vivo potency of small molecules such as ML348 to inhibit APT1 was established in tissue proteomes from mice (*51*). ML348 dose-dependently reduced inclusions and pSer129 of αS in E46K and 3K αS neuronal cultures (*41*) and restored synaptic integrity in cellular and mouse models of Huntington's disease [HD, (*42*)]. Thus, we aimed to test effects of ML348 (structure shown fig. S4B) in mitigating αS-induced synaptic dysfunction.

First, we evaluated pharmacokinetics (PK) of ML348 in 12-month-old C57Bl6 mice after daily intraperitoneally injected doses of 15 or 50 mg/kg for 10 days (fig. S4, A and C). We detected an average of 122 ng/mg in the brain at 15 mg/kg with a dose-dependent raise to 499 ng/ml at 50 mg/kg. The average brain:plasma ratio was ~1:1, demonstrating good brain penetration, in line with

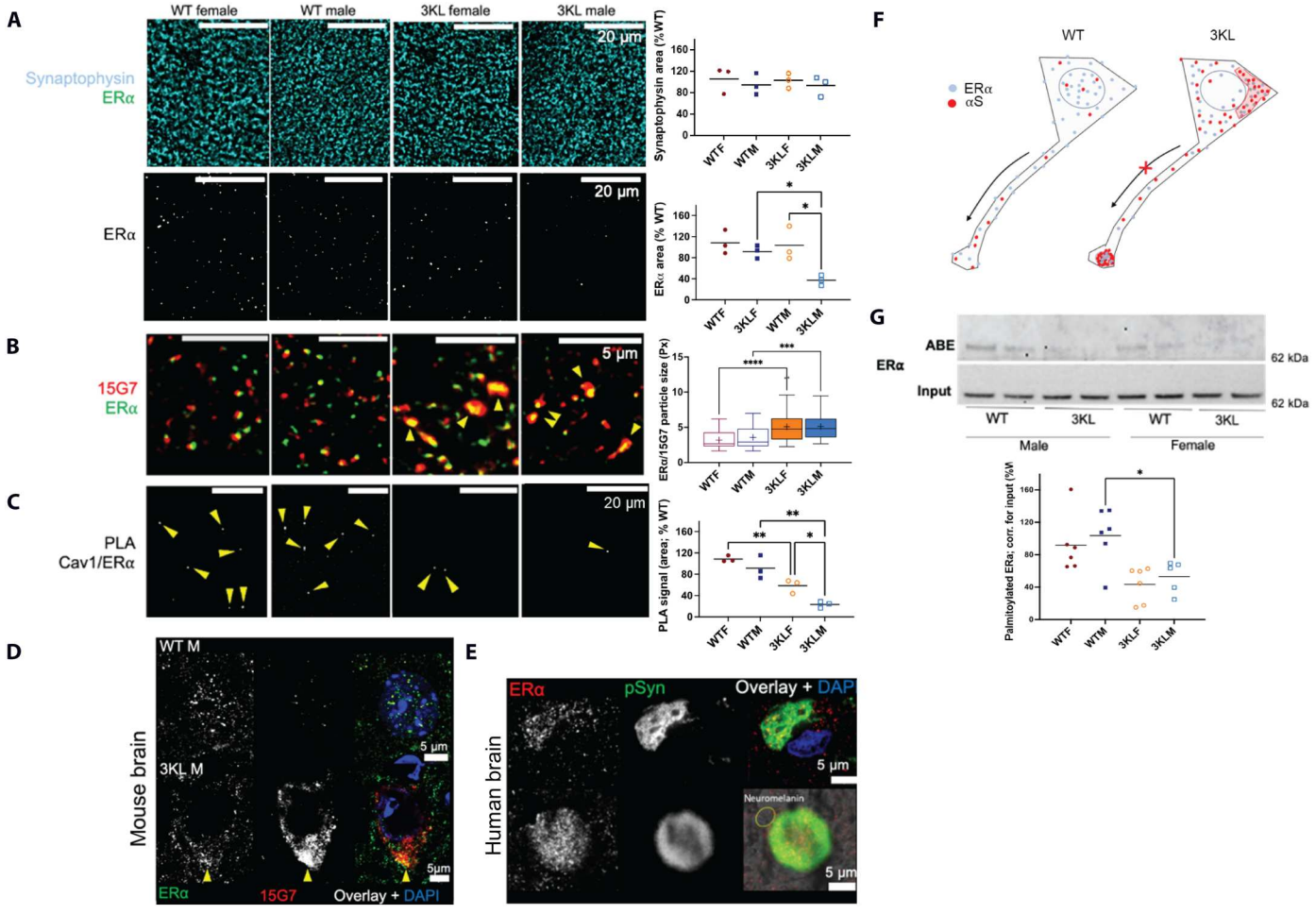

Fig. 3. αS inclusion pathologies affect ERα distribution and palmitoylation. (**A**) Representative images (left) and quantification (right) of synaptophysin$^+$ (top) and ERα + (bottom) puncta in the hippocampal SO of 3KL versus WT males/females and quantification of average %ERα area per mouse (five fields). (**B**) Higher-resolution images of ERα/αS$^+$ in the hippocampal SO of 3KL versus WT males/females and size analysis of colocalizing particles. Arrowheads point to larger-sized ERα/αS foci in 3KL. (**C**) Representative images of ERα:Cav1 PLA in 3KL and WT and quantitation of PLA % area in the hippocampal SO (data points represent average % area per mouse over five subfields). (**D**) Confocal microscopy of cortical neurons labeled for ERα/hu-αS$^+$/4′,6-diamidino-2-phenylindole (DAPI) highlight ERα localization to hu-αS$^+$ inclusions in 3KL (yellow arrowhead) versus nuclear ERα + in WT. (**E**) ERα localization to DLB (top) and PD (bottom) LBs in the transentorhinal cortex (top) and SN (surrounding neuromelanin indicated), respectively. (**F**) Hypothesis: ERα is sequestered into abnormal perinuclear αS$^+$ inclusions and depleted around synapses in 3KL mice (and human PD/DLB). (**G**) WB image of palm-ERα (by ABE assay) in total brain lysates of 3KL versus WT and quantification (n = 5 to 6 per group). (A), (C), and (G) Dot plots show data from individual mice (and median); (B) boxplot based on analyzed fields (16 images per mouse; three mice per group). Statistics by two-way ANOVAs [(A), (C), and (G)] and nonparametric Kruskal-Wallis (B) with Bonferroni/Dunn corrections, respectively (see further table S3); *P < 0.05; **P < 0.01; ***P < 0.001; ****P < 0.0001.

previous observations in HD mice (*42*). To test for oral availability, ML348 was dosed in the drinking water or feeding pellets at 35 and 70 mg/kg (0.35/0.7 g/kg food, respectively) daily for 21 days, and tissue concentrations were compared to the intraperitoneal PK study. Albeit at substantially lower levels, ML348 was detected in the brain after treatment with feeding pellets at 70 mg/kg (average: 23 ng/mg; brain:plasma ratio: ~1:1; fig. S4, A and C). However, ML348 administration in water was associated with substantially lower levels in the brain, likely due to poor water solubility. To confirm that ML348 increased palm-ERα, we performed ABE assays and downstream detection of ERα by WB (similar to Fig. 3G). Because of very low levels of palm-ERα in 3KL mice by WB, we also applied more sensitive mouse ERα ELISA (fig. S4E). Oral treatment resulted in dose-dependent increase of ML348 brain levels [and above those previously reported benefiting HD-like symptoms in mice (*42*)].

To test for potential therapeutic effects of ML348 on behavioral and synaptic impairments in 3K αS mice (Fig. 2, A to C), these mice were treated with ML348 dosed at 0.7 g/kg in feeding pellets for 90 days. The schematic treatment plan and readouts, including cognitive and motor performances during and after treatment, is presented in Fig. 4A. WT mice without these impairments were separately analyzed since we did not expect that enhancing protein palmitoylation would have any effect. Adding ML348 to the feeding pellets did not change overall chow intake of ~2.5 to 3 g/day of WT/3KL mice, indicating a daily dose of approximately 60 to 70 mg/kg, or differences in weight between placebo- and ML348-treated mice (fig. S4F).

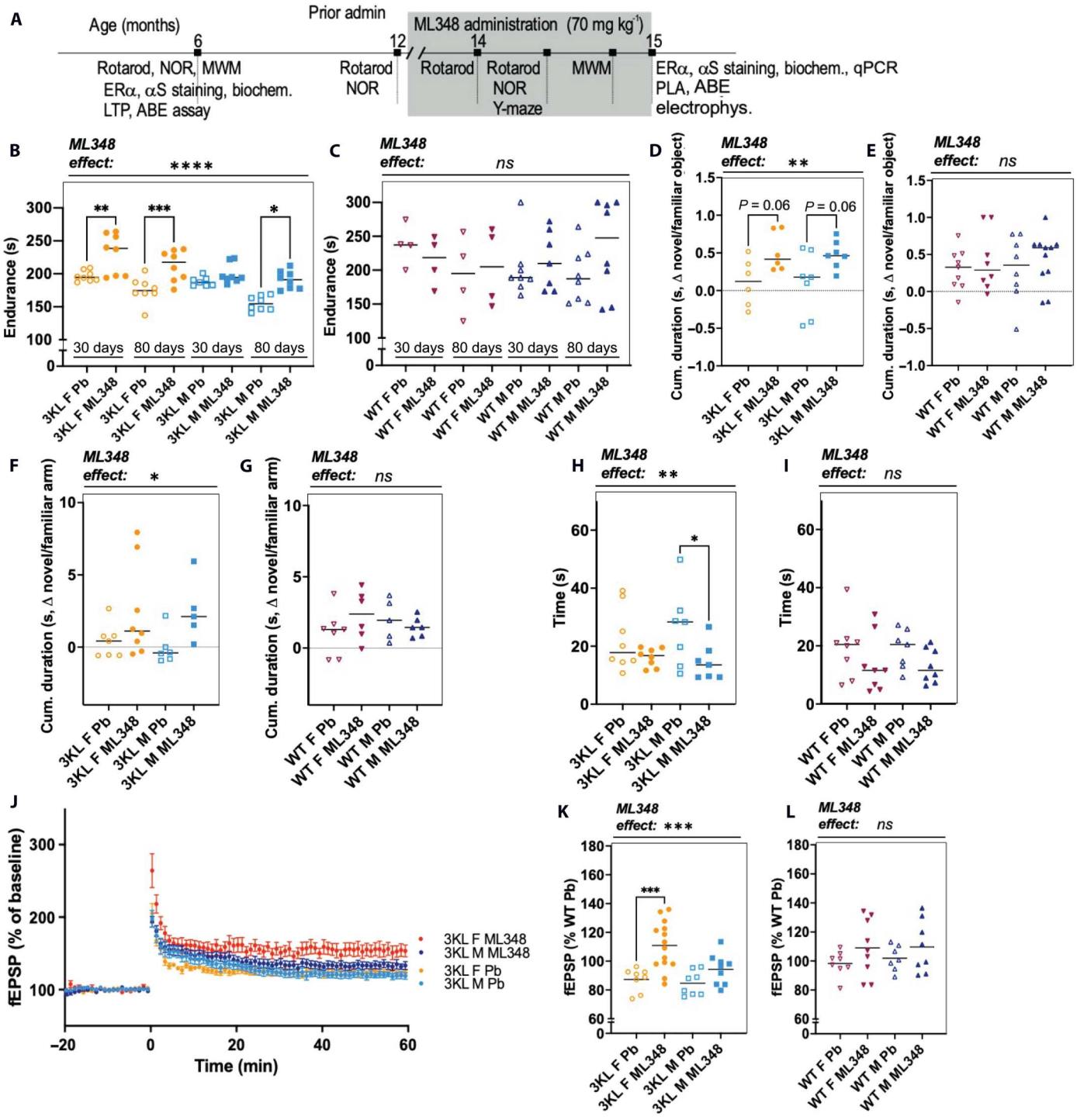

Fig. 4. ML348 ameliorates cognitive deficits and hippocampal synaptic dysfunction in 3KL mice. (**A**) Therapeutic ML348 treatment design, behavioral tests, and readouts in brain tissues. ML348 was applied orally (70 mg kg^{-1}) to symptomatic 3KL or control WT in standard diet pellets. Littermates were treated with placebo. Results of behavioral assessment in placebo- and ML348-treated 3KL or WT mice by (**B** and **C**) rotarod (after 30 and 80 days of treatment), (**D** and **E**) NOR (after 80 days of treatment), (**F** and **G**) Y maze (after 80 days of treatment), and (**H** and **I**) MWM LTM assessment after a 7-day retention interval (after 90 days of treatment). (**J**) Average traces for LTP in acute hippocampal sections of female and male ML348- and placebo-treated 3KL mice. (**K** and **L**) Quantification over the last 5 min of LTP measurements in 3KL or (K) WT (L). Dot plots show data from individual mice (and median) with statistics planned post hoc comparisons for 3KL versus 3KL-ML348 or WT versus WT-ML348. Two-way ANOVA treatment effect over the 3KL/WT treatment cohorts is further indicated above each graph (more details in table S4); ns, non-significant; *P < 0.05;**P < 0.01; ***P < 0.001; ****P < 0.0001.

Fine motor and balancing skills were measured by rotarod after 30 and 80 days of ML348 treatment. At both time points, ML348-treated 3KL males and females both showed improved motor performances compared to placebo (Fig. 4B). Taking measurements at both time points into account, three-way ANOVA revealed a significant effect of treatment ($P < 0.0001$; table S4). While 3KL females performed better than males (reflected by a significant effect of sex; $P < 0.0001$), no treatment × sex interaction effect was found ($P = 0.39$). 3KL females showed significantly improved performance both at 30 days ($P = 0.004$) and 80 days ($P = 0.0008$) of treatment, while the ML348 effect was only significant in 3KL males after 80 days ($P = 0.01$). No significant improvement or deterioration of rotarod performance was observed in WT mice following treatment (Fig. 4C and table S4).

In NOR tests, ML348-treated 3KL mice showed higher discrimination ratios compared to placebo after 80 days of treatment (Fig. 4D), suggesting ameliorated spatial reference memory. A significant overall treatment effect was observed by two-way ANOVA ($P = 0.004$, table S4). Individual post hoc results for comparisons in males/females showed strong trends for better performance in both sexes although nonsignificant after Bonferroni correction (males, $P = 0.06$; females, $P = 0.06$). To validate improved spatial memory by ML348 in 3KL, animals were also tested in a Y maze. Analysis by two-way ANOVA revealed a beneficial ML348 treatment effect in 3KL mice ($F_{1,57} = 7.508$; $P = 0.008$; Fig. 4F). To exclude changes in exploring the mazes, we evaluated ambulatory activity in the NOR/Y maze and found no differences between groups (fig. S4, G and H). No significant treatment effects were found in WT mice for NOR or Y maze performance (Fig. 4, E and G, and table S4).

To evaluate LTM in placebo- and ML348-treated mice, an MWM test was finally conducted during days 80 to 90. No between-group differences were seen during the 4-day training phase (acquisition), in which all (placebo- or ML348-treated 3KL/

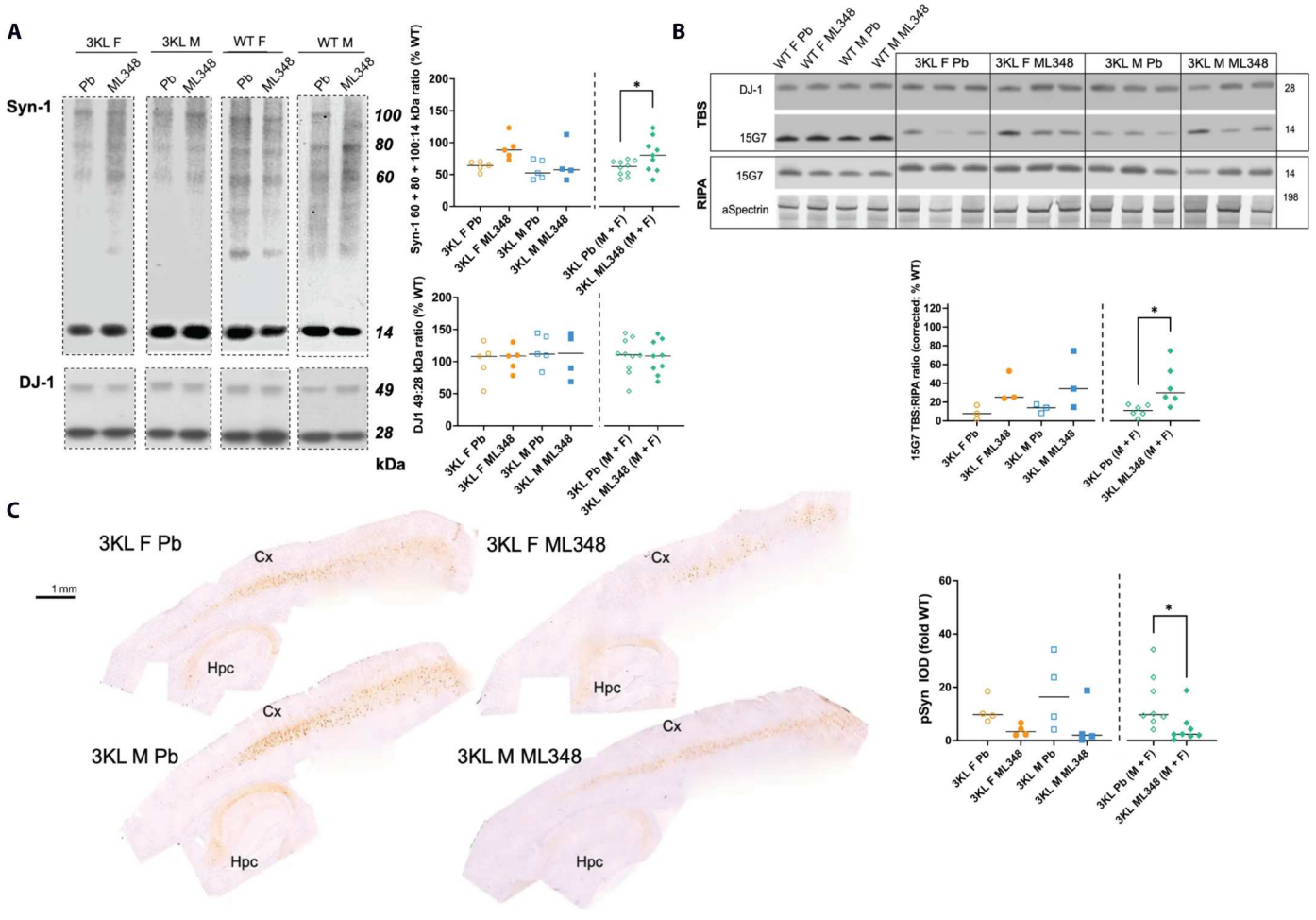

Fig. 5. ML348 ameliorates αS dyshomeostasis and cytopathology in the hippocampus and cortex of 3KL mice. (**A**) Representative WBs for αS (top, ab: Syn-1) and DJ-1 in DSG–cross-linked frontal cortex samples. Graphs, quantification of (60 + 80 + 100 kDa) multimer:(14 kDa) monomer ratios for αS (top) and of dimer/monomer ratios for DJ-1 (full blots for quantification in fig. S7). (**B**) WB detection of αS in sequentially extracted TBS and RIPA hippocampal extracts of placebo (Pb)–treated and ML348-treated 3KL. WT mice are shown as reference. Graph shows quantification of ML348 effects on αS solubility (TBS:RIPA) in 3KL by WB. (**C**) Representative IHC images of pSer129 αS^{+} in ML348- and placebo-treated female and male 3KL mice. Quantification of pSer129 αS IODs in the cortex and hippocampus in sections of ML348- and placebo-treated 3KL mice. Dot plots show data from individual mice (and median). Statistics by two-way ANOVAs. Results of planned post hoc tests with Bonferroni correction are presented (see table S5); *$P < 0.05$.

WT) mice learned to find the hidden platform ($P < 0.05$; fig. S4J, P values in fig. S4K). Two-way ANOVA showed a significant overall treatment effect by ML348 ($P = 0.005$; Fig. 4H and table S4). In particular, after a 7-day retention period, placebo-treated 3KL males took longer to find the hidden platform than ML348-treated 3KL males ($Pf = 0.02$; table S4), which performed more similarly to WT mice. This effect was not paired with changes in swim speed between groups (fig. S4I). Although post hoc results for females were not significant ($P = 0.31$), no significant treatment × sex interaction effect was found ($P = 0.40$). No significant treatment effects were found in WT mice (Fig. 4I and table S4).

We next tested the effect of ML348 treatment on hippocampal synaptic function by measurement of LTP in tissue slices. We observed that LTP levels were significantly elevated in ML348- versus placebo-treated 3KL mice (Fig. 4, J and K; two-way ANOVA treatment effect: $P < 0.0003$). Post hoc test revealed that ML348 effects on LTP were only significant in 3KL females ($P = 0.0002$; $P = 0.23$ in males, table S4), although no significant treatment × sex interaction effect was found ($P = 0.09$; table S4). No significant effect above physiological LTP levels was found in WT mice after ML348 treatment (Fig. 4L). Together, our results suggest that inhibiting de-palmitoylation by ML348 improves cognitive performance and hippocampal synaptic function in 3KL mice.

Oral ML348 treatment alleviates αS dyshomeostasis in 3KL mice

To study whether ML348 synaptic benefits are paralleled by changes in αS homeostasis, we next analyzed αS biochemistry in the hippocampus of placebo- and ML348-treated 3KL male/female mice using WB, and pSer129 αS histopathology in the cortex and hippocampus by IHC (Fig. 5). Given that the behavioral deficits in both 3KL males and females were ameliorated by ML348, without detecting significant treatment × sex interaction effects, we decided to also combine groups in our data analysis and graphing for further evaluation and appreciation of overall treatment effects in our cohort. Results for pooled male/female datasets were compared using a separate t test (male and female placebo-treated 3KL mice versus male and female ML348-treated mice).

Corroborating results at 6 months (Fig. 1A), we observed decreased multimeric relative to monomeric αS species in placebo-treated 3KL compared to WT mice (Fig. 5A and fig. S5A). However, multimer:monomer ratios were higher after ML348 treatment. Two-way ANOVA analysis showed a significant overall treatment effect (treatment effect: $P = 0.04$; details in table S5). Individual post hoc results in placebo- versus ML348-treated 3KL males and females did not reach significance, although a strong trend was observed in 3KL females ($P = 0.07$). No significant treatment × sex interaction effect was found (table S5). Comparison of pooled results from placebo- versus ML348-treated males and females together in a t test supported an overall increase in αS multimerization after ML348 treatment ($t_{17} = 2.22$; $P = 0.04$; Fig. 5A). This effect was not paralleled by changed DJ-1 levels between groups (Fig. 5A) or actin (fig. S5A).

In further support of an improved soluble αS homeostasis, we observed elevated levels of TBS-soluble αS in hippocampal extracts of ML348- versus placebo-treated 3KL mice (Fig. 5B), reflected by higher TBS:RIPA αS ratios (two-way ANOVA ML348 treatment effect: $P = 0.03$; table S5). Although similar trends in 3KL males and females were not significant in these analyses after multiple testing correction (table S5), analysis of pooled male/female data by Student's t test did reach significance ($t_{10} = 2.818$; $P = 0.02$). ML348-treated 3KL mice further exhibited reduced HMW insoluble αS species in hippocampal urea extracts compared to placebo (fig. S5B). We detected an overall significant treatment effect ($F_{1,11} = 12.50$, $P < 0.01$), with similar trends in female ($P = 0.04$) and in male ($P = 0.14$) 3KL mice. We next analyzed pSer129 αS^+ histopathology (Fig. 5C) in cortex and hippocampus of fixed sections. Analysis of pSer129$^+$ αS integrated optical densities showed a significant reduction by ML348 (treatment effect two-way ANOVA; $P = 0.04$; table S5). No significant effects were observed for sex or (treatment × sex) interaction effect (table S5). Overall, we conclude that inhibiting de-palmitoylation by ML348 resulted in subtle but significant amelioration of the soluble αS homeostasis in 3KL male and female mice, reflected by increased αS multimerization, detergent solubility, and a reduction of pSer129$^+$ αS inclusion pathology.

Increased palmitoylation, synaptic availability, and expression levels of ERα by ML348 associate with phenotypic and synaptic benefits in 3KL mice

Since we hypothesized that treatment effects of ML348 would be—at least in part—mediated by increased synaptic availability of palm-ERα, we next conducted electrophysiology in acute hippocampal sections in the presence/absence of the selective ERα antagonist MPP (similar to Fig. 2, H and I). In addition, we applied the PLA for synaptic, palmitoylated ERα:Cav1 association (similar to Fig. 3C) (*47*, *52*), and ABE assays to confirm increase in palm-ERα (similar to Fig. 3G). Last, we assessed *ESR1* transcription levels in the hippocampus of placebo- or ML348-treated mice, as sustained increased brain estradiol in sustained treatment studies was shown to positively correlate with ERα expression level (*50*, *53*).

In line with our expectations, electrophysiology revealed that the increased LTP by ML348 was partially blocked by MPP in 3KL hippocampal sections (Fig. 6A). While only nonsignificant trends for increased LTP levels were detected when the analysis was split in males and females, this became significant when both sexes were pooled together (Fig. 6B; t test, $t_{162} = 3.829$; $P = 0.02$). This result supports a contribution of ERα to LTP improvement by ML348.

To test whether ML348 treatment increased ERα PM availability, we applied the ERα:Cav1 PLA on sections of placebo- versus ML348-treated WT/3KL mice. We observed increased PLA signals in ML348-treated compared to placebo-treated mice (treatment effect two-way ANOVA: $P = 0.001$; post hoc comparisons in males: $P = 0.03$; females $P = 0.02$; Fig. 6B and table S6). In further support of increased association of ERα with the PM, immuno-EM using an antibody against ERα demonstrated numerous PM-associated immunogold particles in ML348-treated mice (fig. S6A); however, this was not further quantified in the present study.

The increased PM distribution of ERα and MPP-dependent LTP increase suggested that ML348 treatment resulted in increased palmitoylation of ERα. To confirm this, we measured palm-ERα by ABE assays in placebo- and ML348-treated 3KL mice. Palm-ERα was detected by ELISAs in ABE fractions, which we validated by WB. ELISA measurements showed an increase in palm-ERα level by ML348 in 3KL mice (Fig. 6C; +45%; two-way ANOVA treatment effect, $P = 0.03$; table S6), albeit stronger in females (+57%, $P = 0.03$) than in males (+24%, not significant). No significant treatment × sex interaction was found ($P = 0.28$). Pooling males/females

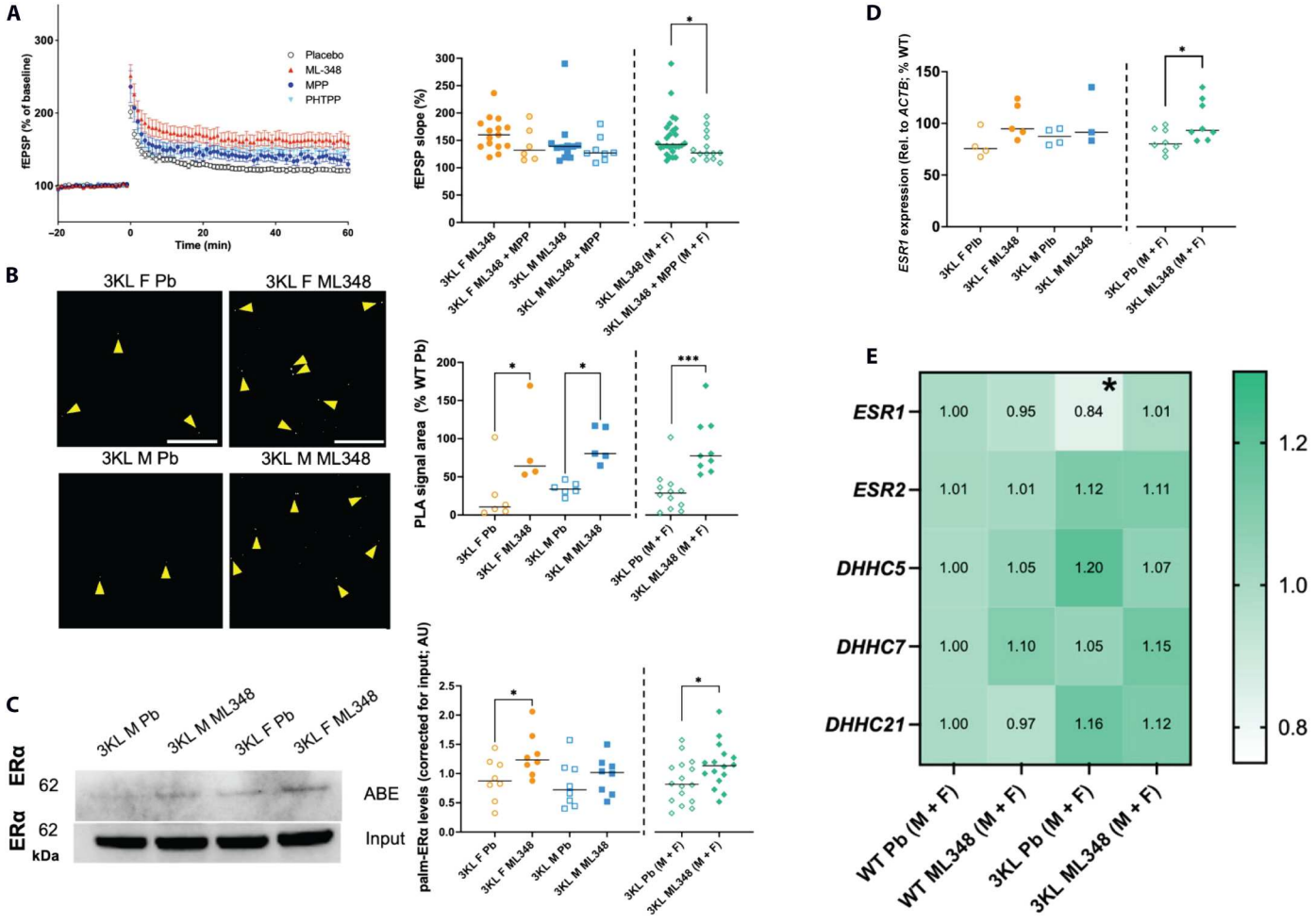

Fig. 6. ERα expression level and palmitoylation contribute to increased hippocampal synaptic function in 15-month-old 3KL mice after ML348. (**A**) Average (M + F) traces of LTP (%fEPSP) in hippocampal sections of placebo- and ML348-treated 3KL males/females and after acute administration of the selective ERα antagonist MPP on sections of ML348-treated mice; (right) quantification of average %fEPSP slopes during the last 5 min of the measurement shown for male/female 3KL and combined (M + F). (**B**) Representative images and quantification of ERα:Cav1 PLA area in hippocampal SO subfields, shown for in 3KL male and female and combined (M + F). Scale bar, 20 μm. (**C**) Representative WB and ELISA-based quantification of palm-ERα in ABE-processed samples of male and female 3KL mice and combined (M + F; quantification in six samples from three mice per group). (**D**) Relative *ESR1* mRNA level in placebo- and ML348-treated WT/3KL mice. (**E**) Heatmap summarizing hippocampal mRNA profiles for ERs and palmitoyl-acyl-transferases (also see fig. S6 for individual scatter blots). Dot plots show data from individual mice (and median). Statistics by two-way ANOVAs. Results of planned post hoc tests with Bonferroni correction are presented (see table S6); *P < 0.05 and ***P < 0.001.

together in a t test showed a significant increase in palm-ERα after ML348 treatment (t_{30} = 2.09; P = 0.05). Of note, we did not discern obvious differences in total palmitoylated proteins in ABE fractions, suggesting more subtle or selective effects (fig. S6B).

As previous reports had indicated ERα transcriptional activity and physiological level depend on palmitoylation (*50*), and ERα can up-regulate its expression levels in a feedforward mechanism (*53*), we next tested mRNA expression of ERs and selected other genes on hippocampal tissues of WT/3KL mice after ML348 treatment at 15 months: We conducted quantitative polymerase chain reaction experiments for *ESR1* (ERα), *ESR2* (Erβ), and the ER-palmitoylating enzymes *DHHC7* and *DHHC21*, as well as *DHHC5*. We found that *ESR1* expression was increased (two-way ANOVA treatment effect: P = 0.04, Fig. 6D and table S6) and more similar to WT levels after ML348 treatment. No significant differences were found for other selected genes (Fig. 6E; given similar trends in males/females, pooled results are presented here for visualization purposes, and results per individual group are provided in fig. S6, C to F). Although we did not observe differences in *DHHCs* transcription levels, this does not rule out that ML348 treatment resulted in changes in its posttranslational modification, which have recently been shown to regulate DHHC activity, for instance, by their phosphorylation, S-acetylation, or ubiquitination (*54*). Of note, we found that overall hippocampal *ESR2* levels were substantially lower when compared to *ESR1* (fig. S6G), which might be in line with previous reports that ERα is transcriptionally more active than Erβ (*45*).

DISCUSSION

Despite increased appreciation of lower prevalence, slower progression, and milder cognitive and neurodegenerative (e.g., atrophy and

preserved DAT availability) features in women with early-stage PD (*55*), the mechanisms that drive this contrast remain insufficiently characterized. Part of these differences could be caused by sexual dimorphism in the homeostasis and processing of αS, a central player in PD pathogenesis. A better understanding of cellular pathways underlying increased resilience against αS-related pathologies in females may provide a basis for the development of protective therapeutic strategies in PD.

Here, we investigated the relationship between estradiol, ER distribution, and the delay of synucleinopathy by female sex we previously reported in PD-like mice (*33*, *34*). In line with clinical PD, we found a delayed onset of phenotypes in female compared to male 3KL mice with moderate overexpression of 3K mutant αS, reproducing our previous findings in a higher-expressing model (*34*). Sequential extractions and intact-cell cross-linking revealed increased αS solubility and multimerization in females compared to males at 6 months, associated with less Ser129p $αS^+$ inclusion pathology (Fig. 1). These differences were not driven by variations in *SNCA* transcript levels. Further phenotyping by behavioral tests and electrophysiology revealed that cognitive phenotypes and synaptic function manifested at a later time point in female 3KL (Fig. 2). In line with stimulating effects of estrogen on synaptic transmission (*39*), elevating brain E2 in 3KL males by DHED treatment or acute E2 administration on sections increased synaptic strength. Previous studies have collectively shown a complex relationship between estrogen and synaptic function and behavior, in which intermediate doses show optimal effects (*44*). Our interpretation of better cognitive function and hippocampal LTP in 3KL male mice, but not WT (Fig. 2), after DHED treatment is that supraphysiological E2 levels are able to compensate for specific pathological insults by 3K αS. Thereby, increased (periodic) estrogen exposure in females may preserve synaptic integrity at early disease stages in female 3KL mice and women with de novo PD (*5*, *6*).

The E2 effect could be blocked using ERα-specific but not ERβ-specific antagonists, suggesting that the prevention of synaptic αS pathologies was mediated by locally available ERα. We found indications that differences in synaptic ERα availability may drive this increased responsiveness due to altered cellular distribution between male and female 3KL (Fig. 3). In particular, more extrasomatic $ERα^+$ immunoreactivity was observed in female versus male 3KL, in line with a previous study (*30*). Furthermore, ERα distribution was affected by progressing 3K αS pathologies, indicating sequestration of ERα into perinuclear $αS^+$ aggregates. The potential relevance for perinuclear ERα arrestation in PD was underlined by the observation of ERα, but not ERβ, localizing to LBs in the PD/DLB brain. The implication of ERα in protective estrogen responses against αS-induced pathologies may have prominent functional and pathogenic implications in conditions of aging and neurodegeneration. Previous studies have suggested benefits for sex hormone treatment in PD (*56*), which may be further improved by brain-selective compounds (*34*, *57*). Moreover, different studies reported that the ERα agonist PTT offers protection against DA neurodegeneration in toxin-based rodent PD models (*58*, *59*). Our findings further substantiate the role of E2 in preserving synaptic plasticity in αS mutant mice, which, our results suggest, relies on the local availability of palm-ERα.

Previous reports indicated that E2 rescues synaptic strength in hippocampal sections of conditional aromatase knockout mice through rapid-acting extranuclear signaling mechanisms (*60*), suggesting that local signaling pathways leading to enhanced synaptic plasticity are operational at the site of synaptic termini. The distribution of ERs is more heterogeneous than previously appreciated, including localization at the PM and around synapses (*46*). The recent identification of ERα′s palmitoylation site (*47*, *48*, *61*, *62*) and synaptosomal membrane binding (*49*, *63*, *64*) has helped in clarifying the role of extranuclear ERs in synaptic plasticity, collectively demonstrating stimulating effects of ERs on LTP formation (*30*). Hippocampal CA1/CA3 neurons are major producers of ERs following E2 exposure (*65*), but ER expression levels decline with age (*66*, *67*), potentially altering the risk on PD. Increased LTP responsiveness to estrogen stimuli in female brain neurons may further be implicated in their enhanced ability for synaptogenesis (*68*) and/or generation of neurites after injury (*69*) or presynaptic vesicle release (*70*). Of note, sex differences in hippocampal LTP have previously been attributed to the X chromosome (*71*) and sex hormones (*44*). In our study, we found no differences in *SNCA* mRNA expression between 3KL males and females, and similar behavioral phenotypes in prepubescent (2-month-old) 3KL mice, supporting a contribution of sex hormones or, alternatively, sex differences in the epigenetic status, which should be addressed in future studies.

Palmitoylation of ERs is pivotal for their transport to and maintenance at the synaptic PM to increase synaptic plasticity (*47*, *72*). We observed that protective E2 effects on αS-induced synaptic deficits in 3KL males were mediated by local ERα, and both ERα palmitoylation and extrasomatic distribution were decreased in 3KL. Previous studies showed that APT inhibition by palmostatin B slowed ERα degradation and prolonged its availability at PMs (*49*, *50*). Moreover, ML348 was shown to reduce αS inclusions and pSer129 in E46K and 3K αS culture models (*41*) and to restore synaptic deficits and mutant nuclear huntingtin accumulation in HD in vitro and in mouse brains (*42*). Inhibiting de-palmitoylation in 3KL mice by ML348 in this study ameliorated motor and cognitive phenotypes, reinstated synaptic plasticity, and increased αS solubility (Figs. 4 and 5). These effects were associated with increased palm-ERα levels and increased PM association. Moreover, we observed a partial blocking of ML348-improved LTP by an ERα antagonist (Fig. 6), all suggesting a contribution of ERα to the ML348 treatment effects.

In accord with previous findings from our laboratory [e.g., (*34*, *73*, *74*)], increased soluble αS homeostasis associated with improved phenotypes in 3K αS-expressing mice. Our observations support that preservation of αS solubility may protect physiological αS function at the synapse. Increasing αS solubility has been explored by various therapeutic approaches, e.g., by preventing formation of insoluble αS species (e.g., using compounds with chaperoning/disaggregating functions) (*75*), or reducing abnormal binding of αS to membranes [e.g., by SCD1 inhibition (*73*, *76*)].

In our current study, we aimed to stimulate synaptic E2 receptiveness by increasing local ERα distribution. A potential mechanism to explain the effects of elevated E2 and extrasomatic ERα on αS-induced synaptic dysfunction could be that E2:ERα signaling counteracts the effects of membrane-associated αS at the synapse; ERα was previously suggested to increase synaptic transmission by mobilizing SVs (*63*), while the opposite—decreased SV mobility and neurotransmitter release—has been shown for αS (*77*, *78*). By stimulating SV flux, synaptic binding of E2 to ERα may release SV from excessive clustering by 3K αS, thereby rendering αS more

soluble. Moreover, previous findings that gamma-synuclein chaperones ERα (*79*) raise the possibility of a direct interaction between ERα and another member of the synuclein family. Other mechanisms underlying protective estrogen signaling could relate to aggregate-resolving features of estrogen/ERα: For instance, ERα has been implicated in autophagy (*34*), by which it could possibly enhance αS aggregate turnover, while E2 was reported to exert disaggregating effects on αS fibrils in vitro (*80*).

Limitations

The results leading to the conclusions of this study were obtained in a humanized mouse model expressing 3K αS, a phenotypic amplification of the E46K mutation (*33*), which models excessive binding of αS monomers to (SV) membranes and downstream pathologies. Despite emerging evidence for a role of αS′s interactions with phospholipid membranes in PD pathogenesis (*76*), our results will have to be corroborated in the context of single αS mutations or sporadic PD. Although synaptic deficits have been demonstrated in various αS-overexpressing mice (*23*), to the best of our knowledge, these studies have so far not reported sex differences in synaptic function. Characterization of sexual dimorphisms and hormonal influences in the onset, severity, and progression of αS-related pathologies (e.g., synaptic dysfunction) in other PD models will aid better translation of our findings to human PD.

In addition, our study is focused on the protective effects of E2, while the effects of other hormones such as follicle-stimulating hormone or testosterone on αS-related pathology have not been addressed. However, previous studies on E2 benefits in PD models by us and others (*34*, *56*–*59*) argue for a role of E2:ER signaling in PD. Furthermore, while our electrophysiology and imaging data suggested that amelioration of αS-induced synaptic impairment by E2 was more prominently mediated by ERα than ERβ (in line with substantially lower hippocampal *ESR2* expression levels), our results do not rule out a (smaller) contribution of ERβ to the DHED/ML348 treatment effects.

A limitation in studying ERα is the unclear specificity of available antibodies. We have addressed this by systematic comparison and selection of antibodies based on their immunoreactivity profiles and by reproducing our main findings using different antibodies. Moreover, using ERα:Cav1 PLA, we developed a method to visualize ERα associated with the PM, which was supported by the observed extranuclear distribution of signal (fig. S3). We found that, although extrasomatic ERα was preserved at 6-month-old female 3KL mice, at this time point, they showed already moderately decreased levels of ERα:Cav1 PLA signals compared to WT and lower ERα palmitoylation levels by WB at this time point. While this could suggest a temporal order in pathological changes ultimately affecting ERα availability and partially masked by higher E2 exposure in females, a direct assessment of palm-ERα distribution was not possible as no antibodies against this specific modified ERα proteoform are currently available.

Our study revealed discrepancies between LTP and memory-associated behaviors in 3K mice, as the significant increase in LTP in 3KL females was not paired by improvements in all cognitive tests. Similar discrepancies have been reported in literature (*81*). A likely explanation for differences in the current study is increased sensitivity of electrophysiology to detect differences in defined hippocampal synaptic pathways, compared to less robust findings in memory-associated behavior, that, however, were still significantly increased by ML348. Future studies would need to define details of the underlying synaptic pathways and whether this disease-modifying treatment could be more efficacious in younger mice with less advanced phenotypes.

ML348 treatment is not specific for ERα but also affects other APT1 substrates. Although we observed an overall ~40% increase of palm-ERα after ML348 treatment in ABE-processed samples (Fig. 6), the increased palmitoylation of other APT-1 substrates (including ERβ) may also have contributed to the ML348 treatment effects, particularly as palmitoylation of various synaptic proteins has been implicated in the formation of LTP [reviewed in (*82*)]. While gross measurements of total palmitoylated protein levels in ABE fractions did not reveal differences between treatment/placebo groups, detailed mapping of changes in the brain palmitome after ML348 treatment could reveal more insights into additional factors contributing to its observed beneficial effects.

Last, our study did not include genetic controls to confirm our hypothesized mechanism of action for ML348. ERα knockout mice and mice that either stimulate or abrogate ERα′s membrane association have been described in literature (*83*, *84*) but show severe developmental effects preventing isolated detailed studies of αS-related pathological phenotypes. Similarly, simultaneous action of two palmitoyl transferases (DHCC7/DHCC21) (*61*) complicates characterization of effects of ERα palmitoylation by genetic approaches in vivo, particularly as sex differences have been previously described for *DHHC7* expression in young adult (70-day-old) mice (*85*, *86*). Although we did not find significant differences in *DHHC* expression in aged mice (fig. S6), this does not rule out a contribution of sex-specific differences in DHHC activity. Genetic crosses of triple-transgenic *DHHC7/DHHC21/SNCA* mutant mice may therefore be required to further dissect the exact impact of (ERα) palmitoylation on synaptic function.

In summary, in addition to the previously described benefit of ML348 on αS aggregation and toxicity in PD-derived neurons (*41*), the results of this study provide additional insights into the relationship of αS solubility, synaptic ERα distribution, and synaptic function. Our study in a moderately overexpressing mouse model of synucleinopathy provides evidence for a role of synaptic ERα availability in female sex protection against αS-induced synaptic phenotypes and suggests that ERα-dependent pathways are able to compensate for specific pathological events by 3K αS (e.g., accumulation of αS monomers with SV membranes), thereby improving cognitive dysfunction in 3KL mice. A better understanding and future modulation of these pathways may provide more individualized, sex-specific therapeutic options in PD and associated disorders.

MATERIALS AND METHODS

Study design

The objective of this study was to examine the impact of sex and estrogen on αS-related synaptic impairment, which is considered an early pathological event in PD. To accomplish this, we studied unique mice with moderate overexpression of a phenotypic amplification of the familial PD-causing E46K αS mutation (3KL mice). Sex differences were studied in 3KL mice at 6 months, a time point associated with the onset of early symptoms and pathology. Between three and five mice for biochemistry, histology, and electrophysiology and six to eight mice for behavior were randomly

selected for each of these experiments. The number of animal numbers per experiment was determined by the investigators based on previous experience or based on pilot studies. For study of treatment effects of recently published APT1 inhibitor ML348, 3KL males and females were randomly assigned to placebo or ML348 treatment groups (n = 7 to 8 per group) for behavioral studies. Within each group, multiple hippocampal sections from three brains per group were studied in electrophysiology experiments and ABE assays, while brains for four of five mice per group were dissected and processed for biochemical analyses and/or histology. The number of mice per group is included in the figure legends.

Experimental animals and ML348 oral treatment

For this study, we used homozygous 3KL αS mutant mice (line no. 3798; JAX, stock 032799) and human WT αS-overexpressing mice (WT, line no. 3877; JAX, stock 414486) or nontransgenic control littermates, as indicated in result text or figure legend. Generation and initial characterization of the mouse lines was described previously (*33*, *34*). In previous studies, WT mice were shown to reveal only very subtle behavioral phenotypes until ~12 months of age (*33*, *34*, *73*, *74*), while 3KL mice developed a progressive motor syndrome with initial symptoms manifesting around the age of 6 months (*33*). All mice were bred and maintained separately at the Hale Building for Transformative Medicine facility in accordance with National Institutes of Health guidelines on use of laboratory animals and an approved protocol (BWH, N2016000314) by Mass General Brigham. Mice were kept in normal 12-hour light/12-hour dark cycles and had free access to food and water. For ML348 treatment, 12-month-old male and female mice were administered the compound (0.7 g of ML348/kg food) accessible ad libitum in standard diet (Research Diets Inc., New Brunswick, NY).

Behavioral tests

All data acquisition and analyses were carried out by an individual blind to the genotype. Six- to fifteen-month-old mice were used for experiments. NOR, Y maze, and MWM testing were tracked with an automated activity detection system, and EthoVision XT software (Noldus) was used to analyze spatial preferences and ambulatory activities (for details on tests, see the Supplementary Materials).

PK parameter analysis for ML348

Analysis for PK parameters of plasma and brain was performed by the Integrated Molecular Structure Education and Research Center (IMSERC) at Northwestern University (Chicago, IL; supported by funding 1-S10-OD021786–01). After administration of ML348 for 10 days (intraperitoneal) (daily at 15 or 50 mg/kg) or 3 weeks (oral in standard diet at 35 or 70 mg/kg), whole blood samples were obtained from cardiac veins for terminal sampling 2 hours after final intraperitoneal dosing into heparinized tubes, and then the brainstems and livers were collected. Brainstems and liver were snap-frozen, and the plasma fraction was immediately separated by centrifugation (3000 rpm, 6 min, 4°C). All tissue was stored at −80°C until liquid chromatography–mass spectrometry analysis.

IHC/IF experiments

Brain was dissected from the skull and postfixed in 4% paraformaldehyde for another 48 hours at 4°C. Brains were cut into 25-μm cryotome sections. After treatment with H_2O_2 to block endogenous peroxidase in the tissue [0.3% in phosphate-buffered saline (PBS), 30 min] and blocking (10% normal goat serum, 1 hour in PBS + 0.05% Tween), sections were incubated overnight at 4°C with anti-pSer129 αS (EP1536Y; Abcam; 1:50,000; RRID: AB_1193226) or ERα (TE111.5D11, Invitrogen, 1:1000; RRID: AB_2101962) diluted in PBS. For ERα staining, sections were additionally blocked in 10% normal mouse serum in PBS for 1 hour. After washing with PBS, the sections were incubated with the respective biotinylated secondary antibodies (1:200 in PBS; Vector Laboratories) and subsequently transferred to ABC solution (1:500 in PBS; Vectastain Elite Kit, Vector Laboratories; RRID: AB_2336819) for 1 hour and visualized with 3,3′-diaminobenzidin (Vector Laboratories; RRID:AB_2336382) as previously described (*33*).

For IF experiments, sections were blocked and permeabilized in 10% normal donkey serum in PBS containing 0.1 to 0.4% Triton X-100 and incubated overnight at 4°C with primary antibodies. For ERα staining, sections were additionally blocked in 10% normal mouse serum in PBS for 1 hour. This was followed by three 5-min washes and incubation with matching fluorophore-conjugated secondary antibodies [1:200 in PBS; Alexa 488, 568, and 647; Abberior STAR 488 RRID (AB_2910107), 580 (RRID:AB_2833016), and 635p (RRID:AB_2893232)] for 2 hours at room temperature. The sections were treated with TrueBlack autofluorescence quencher before mounting using 4′,6-diamidino-2-phenylindole (DAPI)–containing mounting medium (Vectashield) and Prolong Glass antifade mountant (Thermo Fisher Scientific) for confocal and STED experiments, respectively.

Proximity ligation assay

In situ PLA (Duolink) was performed in accordance with the manufacturer's protocol. Briefly, samples were permeabilized using 0.3%Triton X-100 in PBS, further containing 5% normal mouse serum. After this, sections were blocked using Duolink blocking solution for 1 hour at 37°C. Sections were incubated overnight in diluted primary antibodies against ERα (TE111.5D11, Invitrogen, RRID: AB_2101962, 1:100 in Duolink Antibody Diluent) and Cav1 (no. D46G3; RRID:AB_2275453, Cell Signaling Technology; 1:100 in Duolink Antibody Diluent) at 4°C. After washing, the sections were incubated with Duolink PLA probes (goat anti-mouse PLUS; goat anti-rabbit MINUS) for 1 hour at 37°C, after which, ligation and amplification steps were performed according to the manufacturer's protocols (incubation times: 30 and 90 min at 37°C, respectively). Sections were washed and treated with TrueBlack autofluorescence quencher (Biotium) before mounting using DAPI-containing mounting medium (Vectashield).

Confocal and STED microscopy

Confocal microscopy was conducted with a Leica TCS SP8 STED 3× microscope and LASX navigator software (Leica). Images were acquired using an HC PL APO CS2 63× 1.4 numerical aperture oil objective lens in combination with highly sensitive hybrid (HyD) detectors in photocounting mode. Resolution was set to a pixel size of 50 nm by 50 nm or 20 nm by 20 nm for confocal and STED imaging, respectively. After scanning, deconvolution was performed using CMLE (for confocal images) and GMLE algorithms (for STED images) in Huygens Professional software (Scientific Volume Imaging; Huygens, the Netherlands).

Image processing and analysis

Processing and analyses for confocal images were done in Fiji ImageJ by an experimenter blinded to the conditions. In short, images belonging to one experiment were thresholded using the same preset FIJI algorithm. The FIJI plugin "Colocalization Highlighter" was used to analyze colocalization by creating a mask of overlapped pixels. The number or sizes or percentage area of the colocalized pixels on the resultant 8-bit images was quantified using the FIJI "Analyze particle" function. Images for WB quantification were only adjusted for contrast and brightness.

ABE assay

Tissue homogenates from mouse brain samples were analyzed by ABE assays as previously described, with minor modifications (*41*, *87*, *88*). Samples were homogenized in lysis buffer (50 mM tris, 150 NaCl, 1 mM EDTA, 1% Triton X-100, 0.1% SDS, and 0.1% sodium deoxycholate, supplemented with protease inhibitors) using an IKA Microstar 7.5 stirrer at 700 rpm with 35 strokes in a 5-ml Teflon-coated radially serrated tissue grinder (DWK/Wheaton #357974). Following protein measurement by the Bradford method, proteins at a concentration of 1 mg/ml of buffer were treated with 10 mM NEM for 20 min at 37°C in buffer containing 50 mM tris and 2.5% SDS to ensure protein denaturation. Acetone precipitation was performed to remove unreacted NEM. Following this, protein was re-suspended in 240 µl of buffer containing 4% SDS, 50 mM tris, 5 mM EDTA, and 0.8% Triton X-100. Then, 560 µl of 1 M hydroxylamine solution, pH 7.4 was added, along with 200 µl of 2 mM biotin-HPDP (Pierce PI21341) for a final concentration of 0.56 M hydroxylamine and 0.8 mM biotin-HPDP. Samples were incubated with end-over-end rotation for 1 hour, then desalted to remove unreacted biotin-HPDP using a Zeba 7K MW cut-off desalting column (Pierce #89892). To enhance removal of excess biotin-HPDP and to concentrate protein, samples were then acetone precipitated as before. Biotinylated proteins were purified using neutravidin agarose (Pierce # 29201), eluted with 1% β-mercapto-ethanol, separated by SDS-PAGE, and analyzed by WB or ERα ELISA.

ERα ELISA

The brain concentration of ERα was measured using a mouse-specific ELISA kit (LSBio, LS-F22233; range, 0.3 to 20 ng/ml) according to the manufacturer's instruction. The lysed samples were diluted in TBS (1:100) or RIPA (1:75) buffer and normalized to the total protein concentration (Pierce bicinchoninic acid protein assay; Thermo Fisher Scientific).

Quantitative and statistical analysis

Details regarding each statistical test, biological sample size (n) and P value can be found in the corresponding figure legends and in Results. Dot plots with median were used to visualize the individual data points, unless otherwise indicated. The large majority of datasets did not show deviations for normality. Comparisons between 3KL/WT males and females at 6 months were done using two-way ANOVAs to test the effects of genotype and sex (and also interactions between them), while in behavioral tests and LTP measurements, the effect of time was also studied (three-way ANOVAs). Post hoc analysis was done using planned pairwise comparisons (specified in the Supplementary tables) and adjusted by Bonferroni corrections. In the ML348 treatment studies, two-way ANOVA analyses were done on data from symptomatic 3KL mice to analyze the ML348 effect on their deficits. In addition to the treatment effect (placebo versus ML348), sex effects and interaction between them were analyzed. Post hoc analysis was done using planned pairwise comparisons (specified in the Supplementary tables) and adjusted by Bonferroni corrections. In case of deviation from normality, Kruskal-Wallis tests were used to test between-group differences, followed by post hoc tests adjusted by Dunn's correction. Data from statistical tests are presented in the Supplementary tables to Figs. 1 to 6 (tables S1 to S6). Behavioral tests, histological and ultrastructural imaging, and electrophysiology were routinely performed blind to the conditions of the experiments. For free (non-forced) exploration studies in the NOR and Y maze test, a planned ROUT (Q = 1%) test was used to identify outliers defined per absence of exploration that exceeded >30% of the testing time period. Identified outlier in NOR (Fig. 4D): n = 1 3KL-F, n = 2 WT-F, and n = 2 WT-M. Identified outlier in the Y maze (Fig. 4E: n = 2 3KL-M). All statistical analyses were performed using GraphPad Prism 9. Behavioral tests, histological and ultrastructural imaging, and electrophysiology were routinely performed blind to the conditions of the experiments. For free (non-forced) exploration studies in the NOR and Y maze test, a ROUT (Q = 1%) test was used to identify outliers defined per absence of exploration that exceeded >30% of the testing time period. Identified outlier in NOR (Fig. 4D): n = 1 3KL-F, n = 2 WT-F, and n = 2 WT-M. Identified outlier in the Y maze (Fig. 4E: n = 2 3KL-M). All statistical analyses were performed using GraphPad Prism 9.

Supplementary Materials

This PDF file includes:

Supplementary Materials and Methods
Tables S1 to S6
Figs. S1 to S6
References

REFERENCES AND NOTES

1. J. Oltra, C. Uribe, A. Campabadal, A. Inguanzo, G. C. Monte-Rubio, M. J. Marti, Y. Compta, F. Valldeoriola, C. Junque, B. Segura, Sex differences in brain and cognition in *de novo* Parkinson's disease. *Front. Aging Neurosci.* **13**, 791532 (2022).
2. T. H. Reekes, C. I. Higginson, C. R. Ledbetter, N. Sathivadivel, R. M. Zweig, E. A. Disbrow, Sex specific cognitive differences in Parkinson disease. *NPJ Parkinson's dis.* **6**, 7 (2020).
3. S. K. Yadav, N. Kathiresan, S. Mohan, G. Vasileiou, A. Singh, D. Kaura, E. R. Melhem, R. K. Gupta, E. Wang, F. M. Marincola, A. Borthakur, M. Haris, Gender-based analysis of cortical thickness and structural connectivity in Parkinson's disease. *J. Neurol.* **263**, 2308–2318 (2016).
4. C. Tremblay, N. Abbasi, Y. Zeighami, Y. Yau, M. Dadar, S. Rahayel, A. Dagher, Sex effects on brain structure in de novo Parkinson's disease: A multimodal neuroimaging study. *Brain.* **143**, 3052–3066 (2020).
5. C. A. Haaxma, B. R. Bloem, G. F. Borm, W. J. G. Oyen, K. L. Leenders, S. Eshuis, J. Booij, D. E. Dluzen, M. W. Horstink, Gender differences in Parkinson's disease. *J. Neurol. Neurosurg. Psychiatry* **78**, 819–824 (2007).
6. V. Kaasinen, J. Joutsa, T. Noponen, J. Johansson, M. Seppanen, Effects of aging and gender on striatal and extrastriatal [123I]FP-CIT binding in Parkinson's disease. *Neurobiol. Aging* **36**, 1757–1763 (2015).
7. D. Colombo, G. Abbruzzese, A. Antonini, P. Barone, G. Bellia, F. Franconi, L. Simoni, M. Attar, E. Zagni, S. Haggiag, F. Stocchi, The "gender factor" in wearing-off among patients with Parkinson's disease: A post hoc analysis of DEEP study. *ScientificWorldJournal* **2015**, 787451 (2015).
8. P. Martinelli, M. Contin, C. Scaglione, R. Riva, F. Albani, A. Baruzzi, Levodopa pharmacokinetics and dyskinesias: Are there sex-related differences? *Neurol. Sci.* **24**, 192–193 (2003).

9. P. Ragonese, M. D'Amelio, G. Salemi, P. Aridon, M. Gammino, A. Epifanio, L. Morgante, G. Savettieri, Risk of Parkinson disease in women: Effect of reproductive characteristics. *Neurology* **62**, 2010–2014 (2004).
10. P. Ragonese, M. D'Amelio, G. Callari, G. Salemi, L. Morgante, G. Savettieri, Age at menopause predicts age at onset of Parkinson's disease. *Mov. Disord.* **21**, 2211–2214 (2006).
11. W. A. Rocca, B. R. Grossardt, D. M. Maraganore, The long-term effects of oophorectomy on cognitive and motor aging are age dependent. *Neurodegener. Dis.* **5**, 257–260 (2008).
12. K. L. Tsang, S. L. Ho, S. K. Lo, Estrogen improves motor disability in parkinsonian postmenopausal women with motor fluctuations. *Neurology* **54**, 2292–2298 (2000).
13. P. J. Blanchet, J. Fang, K. Hyland, L. A. Arnold, M. M. Mouradian, T. N. Chase, Short-term effects of high-dose 17beta-estradiol in postmenopausal PD patients: A crossover study. *Neurology* **53**, 91–95 (1999).
14. R. V. Dye, K. J. Miller, E. J. Singer, A. J. Levine, Hormone replacement therapy and risk for neurodegenerative diseases. *Int J Alzheimers Dis* **2012**, 258454 (2012).
15. J. E. Rossouw, G. L. Anderson, R. L. Prentice, A. Z. LaCroix, C. Kooperberg, M. L. Stefanick, R. D. Jackson, S. A. Beresford, B. V. Howard, K. C. Johnson, J. M. Kotchen, J. Ockene; Writing Group for the Women's Health Initiative Investigators, Risks and benefits of estrogen plus progestin in healthy postmenopausal women: Principal results From the Women's Health Initiative randomized controlled trial. *JAMA* **288**, 321–333 (2002).
16. M. G. Spillantini, R. A. Crowther, R. Jakes, M. Hasegawa, M. Goedert, alpha-Synuclein in filamentous inclusions of Lewy bodies from Parkinson's disease and dementia with lewy bodies. *Proc. Natl. Acad. Sci. U.S.A.* **95**, 6469–6473 (1998).
17. D. Sulzer, R. H. Edwards, The physiological role of α-synuclein and its relationship to Parkinson's disease. *J. Neurochem.* **150**, 475–486 (2019).
18. J. Burre, The synaptic function of α-synuclein. *J. Parkinsons Dis.* **5**, 699–713 (2015).
19. J. Burre, M. Sharma, T. C. Sudhof, Cell biology and pathophysiology of α-synuclein. *Cold Spring Harb. Perspect. Med.* **8**, a024091 (2018).
20. L. Wang, U. Das, D. A. Scott, Y. Tang, P. J. McLean, S. Roy, α-Synuclein multimers cluster synaptic vesicles and attenuate recycling. *Curr. Biol.* **24**, 2319–2326 (2014).
21. T. Logan, J. Bendor, C. Toupin, K. Thorn, R. H. Edwards, α-Synuclein promotes dilation of the exocytotic fusion pore. *Nat. Neurosci.* **20**, 681–689 (2017).
22. J. C. Bridi, F. Hirth, Mechanisms of α-Synuclein induced synaptopathy in Parkinson's disease. *Front. Neurosci.* **12**, 80 (2018).
23. V. Ghiglieri, V. Calabrese, P. Calabresi, Alpha-synuclein: From early synaptic dysfunction to neurodegeneration. *Front. Neurol.* **9**, 295 (2018).
24. T. Schirinzi, G. Madeo, G. Martella, M. Maltese, B. Picconi, P. Calabresi, A. Pisani, Early synaptic dysfunction in Parkinson's disease: Insights from animal models. *Mov. Disord.* **31**, 802–813 (2016).
25. S. H. Shahmoradian, A. J. Lewis, C. Genoud, J. Hench, T. E. Moors, P. P. Navarro, D. Castano-Diez, G. Schweighauser, A. Graff-Meyer, K. N. Goldie, R. Sutterlin, E. Huisman, A. Ingrassia, Y. Gier, A. J. M. Rozemuller, J. Wang, A. Paepe, J. Erny, A. Staempfli, J. Hoernschemeyer, F. Grosseruschkamp, D. Niedieker, S. F. El-Mashtoly, M. Quadri, I. W. F. J. Van, V. Bonifati, K. Gerwert, B. Bohrmann, S. Frank, M. Britschgi, H. Stahlberg, W. D. J. Van de Berg, M. E. Lauer, Lewy pathology in Parkinson's disease consists of crowded organelles and lipid membranes. *Nat. Neurosci.* **22**, 1099–1109 (2019).
26. A. McCormack, D. J. Keating, N. Chegeni, A. Colella, J. J. Wang, T. Chataway, Abundance of synaptic vesicle-related proteins in alpha-synuclein-containing protein inclusions suggests a targeted formation mechanism. *Neurotox. Res.* **35**, 883–897 (2019).
27. H. Hall, S. Reyes, N. Landeck, C. Bye, G. Leanza, K. Double, L. Thompson, G. Halliday, D. Kirik, Hippocampal Lewy pathology and cholinergic dysfunction are associated with dementia in Parkinson's disease. *Brain.* **137**, 2493–2508 (2014).
28. H. I. Hurtig, J. Q. Trojanowski, J. Galvin, D. Ewbank, M. L. Schmidt, V. M. Lee, C. M. Clark, G. Glosser, M. B. Stern, S. M. Gollomp, S. E. Arnold, Alpha-synuclein cortical Lewy bodies correlate with dementia in Parkinson's disease. *Neurology* **54**, 1916–1921 (2000).
29. T. E. Moors, D. Mona, S. Luehe, G. Duran-Pacheco, L. Spycher, O. Mundigl, K. Kaluza, S. Huber, M. N. Hug, T. Kremer, M. Ritter, S. Dziadek, G. Dernick, W. D. J. van de Berg, M. Britschgi, Multi-platform quantitation of alpha-synuclein human brain proteoforms suggests disease-specific biochemical profiles of synucleinopathies. *Acta Neuropathol. Commun.* **10**, 82 (2022).
30. W. Wang, A. A. Le, B. Hou, J. C. Lauterborn, C. D. Cox, E. R. Levin, G. Lynch, C. M. Gall, Memory-related synaptic plasticity is sexually dimorphic in rodent hippocampus. *J. Neurosci.* **38**, 7935–7951 (2018).
31. U. Dettmer, A. J. Newman, F. Soldner, E. S. Luth, N. C. Kim, V. E. von Saucken, J. B. Sanderson, R. Jaenisch, T. Bartels, D. Selkoe, Parkinson-causing α-synuclein missense mutations shift native tetramers to monomers as a mechanism for disease initiation. *Nat. Commun.* **6**, 7314 (2015).
32. U. Dettmer, A. J. Newman, V. E. von Saucken, T. Bartels, D. Selkoe, KTKEGV repeat motifs are key mediators of normal α-synuclein tetramerization: Their mutation causes excess monomers and neurotoxicity. *Proc. Natl. Acad. Sci. U.S.A.* **112**, 9596–9601 (2015).
33. S. Nuber, M. Rajsombath, G. Minakaki, J. Winkler, C. P. Muller, M. Ericsson, B. Caldarone, U. Dettmer, D. J. Selkoe, Abrogating native α-synuclein tetramers in mice causes a L-DOPA-responsive motor syndrome closely resembling Parkinson's disease. *Neuron* **100**, 75–90. e5 (2018).
34. M. M. Rajsombath, A. Y. Nam, M. Ericsson, S. Nuber, Female sex and brain-selective estrogen benefit α-synuclein tetramerization and the PD-like motor syndrome in 3K transgenic mice. *J. Neurosci.* **39**, 7628–7640 (2019).
35. L. Prokai, V. Nguyen, S. Szarka, P. Garg, G. Sabnis, H. A. Bimonte-Nelson, K. J. McLaughlin, J. S. Talboom, C. D. Conrad, P. J. Shughrue, T. D. Gould, A. Brodie, I. Merchenthaler, P. Koulen, K. Prokai-Tatrai, The prodrug DHED selectively delivers 17beta-estradiol to the brain for treating estrogen-responsive disorders. *Sci. Transl. Med.* **7**, 297ra113 (2015).
36. B. Liu, D. E. Dluzen, Oestrogen and nigrostriatal dopaminergic neurodegeneration: Animal models and clinical reports of Parkinson's disease. *Clin. Exp. Pharmacol. Physiol.* **34**, 555–565 (2007).
37. G. E. Gillies, S. McArthur, Estrogen actions in the brain and the basis for differential action in men and women: A case for sex-specific medicines. *Pharmacol. Rev.* **62**, 155–198 (2010).
38. G. E. Gillies, S. McArthur, Independent influences of sex steroids of systemic and central origin in a rat model of Parkinson's disease: A contribution to sex-specific neuroprotection by estrogens. *Horm. Behav.* **57**, 23–34 (2010).
39. Y. Hara, E. M. Waters, B. S. McEwen, J. H. Morrison, Estrogen effects on cognitive and synaptic health over the lifecourse. *Physiol. Rev.* **95**, 785–807 (2015).
40. L. Fonseca-Ornelas, T. Viennet, M. Rovere, H. Jiang, L. Liu, S. Nuber, M. Ericsson, H. Arthanari, D. J. Selkoe, Altered conformation of α-synuclein drives dysfunction of synaptic vesicles in a synaptosomal model of Parkinson's disease. *Cell Rep.* **36**, 109333 (2021).
41. G. P. H. Ho, N. Ramalingam, T. Imberdis, E. C. Wilkie, U. Dettmer, D. J. Selkoe, Upregulation of cellular palmitoylation mitigates α-synuclein accumulation and neurotoxicity. *Mov. Disord.* **36**, 348–359 (2021).
42. A. Virlogeux, C. Scaramuzzino, S. Lenoir, R. Carpentier, M. Louessard, A. Genoux, P. Lino, M. V. Hinckelmann, A. L. Perrier, S. Humbert, F. Saudou, Increasing brain palmitoylation rescues behavior and neuropathology in Huntington disease mice. *Sci. Adv.* **7**, eabb0799 (2021).
43. F. E. Harrison, A. H. Hosseini, M. P. McDonald, Endogenous anxiety and stress responses in water maze and Barnes maze spatial memory tasks. *Behav. Brain Res.* **198**, 247–251 (2009).
44. P. A. S. Sheppard, E. Choleris, L. A. M. Galea, Structural plasticity of the hippocampus in response to estrogens in female rodents. *Mol. Brain* **12**, 22 (2019).
45. L. A. Bean, L. Ianov, T. C. Foster, Estrogen receptors, the hippocampus, and memory. *Neuroscientist.* **20**, 534–545 (2014).
46. T. A. Milner, B. S. McEwen, S. Hayashi, C. J. Li, L. P. Reagan, S. E. Alves, Ultrastructural evidence that hippocampal alpha estrogen receptors are located at extranuclear sites. *J. Comp. Neurol.* **429**, 355–371 (2001).
47. F. Acconcia, P. Ascenzi, G. Fabozzi, P. Visca, M. Marino, S-palmitoylation modulates human estrogen receptor-alpha functions. *Biochem. Biophys. Res. Commun.* **316**, 878–883 (2004).
48. M. Marino, P. Ascenzi, F. Acconcia, S-palmitoylation modulates estrogen receptor alpha localization and functions. *Steroids* **71**, 298–303 (2006).
49. N. Tabatadze, T. Smejkalova, C. S. Woolley, Distribution and posttranslational modification of synaptic ERα in the adult female rat hippocampus. *Endocrinology* **154**, 819–830 (2013).
50. P. La Rosa, V. Pesiri, G. Leclercq, M. Marino, F. Acconcia, Palmitoylation regulates 17β-estradiol-induced estrogen receptor-α degradation and transcriptional activity. *Mol. Endocrinol.* **26**, 762–774 (2012).
51. A. Adibekian, B. R. Martin, J. W. Chang, K. L. Hsu, K. Tsuboi, D. A. Bachovchin, A. E. Speers, S. J. Brown, T. Spicer, V. Fernandez-Vega, J. Ferguson, P. S. Hodder, H. Rosen, B. F. Cravatt, Confirming target engagement for reversible inhibitors in vivo by kinetically tuned activity-based probes. *J. Am. Chem. Soc.* **134**, 10345–10348 (2012).
52. J. I. Luoma, M. I. Boulware, P. G. Mermelstein, Caveolin proteins and estrogen signaling in the brain. *Mol. Cell. Endocrinol.* **290**, 8–13 (2008).
53. T. C. Foster, Role of estrogen receptor alpha and beta expression and signaling on cognitive function during aging. *Hippocampus* **22**, 656–669 (2012).
54. F. Zmuda, L. H. Chamberlain, Regulatory effects of post-translational modifications on zDHHC S-acyltransferases. *J. Biol. Chem.* **295**, 14640–14652 (2020).
55. G. E. Gillies, I. S. Pienaar, S. Vohra, Z. Qamhawi, Sex differences in Parkinson's disease. *Front. Neuroendocrinol.* **35**, 370–384 (2014).
56. K. L. Tsang, H. Jiang, D. B. Ramsden, S. L. Ho, The use of estrogen in the treatment of Parkinson's disease. *Parkinsonism Relat. Disord.* **8**, 133–137 (2001).
57. N. Thadathil, J. Xiao, R. Hori, S. E. Alway, M. M. Khan, Brain selective estrogen treatment protects dopaminergic neurons and preserves behavioral function in MPTP-induced mouse model of Parkinson's disease. *J. Neuroimmune Pharmacol.* **16**, 667–678 (2021).
58. M. D'Astous, M. Morissette, T. Di Paolo, Effect of estrogen receptor agonists treatment in MPTP mice: Evidence of neuroprotection by an ER alpha agonist. *Neuropharmacology* **47**, 1180–1188 (2004).

59. A. M. Baraka, A. A. Korish, G. A. Soliman, H. Kamal, The possible role of estrogen and selective estrogen receptor modulators in a rat model of Parkinson's disease. *Life Sci.* **88**, 879–885 (2011).
60. Y. Lu, G. R. Sareddy, J. Wang, R. Wang, Y. Li, Y. Dong, Q. Zhang, J. Liu, J. C. O'Connor, J. Xu, R. K. Vadlamudi, D. W. Brann, Neuron-derived estrogen regulates synaptic plasticity and memory. *J. Neurosci.* **39**, 2792–2809 (2019).
61. A. Pedram, M. Razandi, R. J. Deschenes, E. R. Levin, DHHC-7 and -21 are palmitoylacyltransferases for sex steroid receptors. *Mol. Biol. Cell* **23**, 188–199 (2012).
62. A. Pedram, M. Razandi, R. C. Sainson, J. K. Kim, C. C. Hughes, E. R. Levin, A conserved mechanism for steroid receptor translocation to the plasma membrane. *J. Biol. Chem.* **282**, 22278–22288 (2007).
63. S. A. Hart, M. A. Snyder, T. Smejkalova, C. S. Woolley, Estrogen mobilizes a subset of estrogen receptor-alpha-immunoreactive vesicles in inhibitory presynaptic boutons in hippocampal CA1. *J. Neurosci.* **27**, 2102–2111 (2007).
64. M. I. Boulware, J. D. Heisler, K. M. Frick, The memory-enhancing effects of hippocampal estrogen receptor activation involve metabotropic glutamate receptor signaling. *J. Neurosci.* **33**, 15184–15194 (2013).
65. R. D. Romeo, J. B. McCarthy, A. Wang, T. A. Milner, B. S. McEwen, Sex differences in hippocampal estradiol-induced N-methyl-D-aspartic acid binding and ultrastructural localization of estrogen receptor-alpha. *Neuroendocrinology* **81**, 391–399 (2005).
66. M. M. Adams, S. E. Fink, R. A. Shah, W. G. Janssen, S. Hayashi, T. A. Milner, B. S. McEwen, J. H. Morrison, Estrogen and aging affect the subcellular distribution of estrogen receptor-alpha in the hippocampus of female rats. *J. Neurosci.* **22**, 3608–3614 (2002).
67. R. D. Mehra, K. Sharma, C. Nyakas, U. Vij, Estrogen receptor alpha and beta immunoreactive neurons in normal adult and aged female rat hippocampus: A qualitative and quantitative study. *Brain Res.* **1056**, 22–35 (2005).
68. L. Fester, J. Prange-Kiel, L. Zhou, B. V. Blittersdorf, J. Bohm, H. Jarry, M. Schumacher, G. M. Rune, Estrogen-regulated synaptogenesis in the hippocampus: Sexual dimorphism in vivo but not in vitro. *J. Steroid Biochem. Mol. Biol.* **131**, 24–29 (2012).
69. S. McArthur, G. E. Gillies, Peripheral vs. central sex steroid hormones in experimental Parkinson's disease. *Front Endocrinol (Lausanne)* **2**, 82 (2011).
70. T. Smejkalova, C. S. Woolley, Estradiol acutely potentiates hippocampal excitatory synaptic transmission through a presynaptic mechanism. *J. Neurosci.* **30**, 16137–16148 (2010).
71. S. R. Ocanas, V. A. Ansere, K. B. Tooley, N. Hadad, A. J. Chucair-Elliott, D. R. Stanford, S. Rice, B. Wronowski, K. D. Pham, J. M. Hoffman, S. N. Austad, M. B. Stout, W. M. Freeman, Differential regulation of mouse hippocampal gene expression sex differences by chromosomal content and gonadal sex. *Mol. Neurobiol.* **59**, 4669–4702 (2022).
72. J. Meitzen, J. I. Luoma, M. I. Boulware, V. L. Hedges, B. M. Peterson, K. Tuomela, K. A. Britson, P. G. Mermelstein, Palmitoylation of estrogen receptors is essential for neuronal membrane signaling. *Endocrinology* **154**, 4293–4304 (2013).
73. S. Nuber, A. Y. Nam, M. M. Rajsombath, H. Cirka, X. Hronowski, J. Wang, K. Hodgetts, L. S. Kalinichenko, C. P. Muller, V. Lambrecht, J. Winkler, A. Weihofen, T. Imberdis, U. Dettmer, S. Fanning, D. J. Selkoe, A stearoyl-coenzyme a desaturase inhibitor prevents multiple Parkinson disease phenotypes in α-synuclein mice. *Ann. Neurol.* **89**, 74–90 (2021).
74. S. Nuber, C. Y. Chung, D. F. Tardiff, P. A. Bechade, T. D. McCaffery, K. Shimanaka, J. Choi, B. Chang, W. Raja, E. Neve, C. Burke, X. Jiang, P. Xu, V. Khurana, U. Dettmer, S. Fanning, K. J. Rhodes, D. J. Selkoe, R. H. Scannevin, A brain-penetrant stearoyl-CoA desaturase inhibitor reverses α-synuclein toxicity. *Neurotherapeutics* **19**, 1018–1036 (2022).
75. D. Ebrahimi-Fakhari, L. J. Saidi, L. Wahlster, Molecular chaperones and protein folding as therapeutic targets in Parkinson's disease and other synucleinopathies. *Acta Neuropathol. Commun.* **1**, 79 (2013).
76. S. Fanning, D. Selkoe, U. Dettmer, Parkinson's disease: Proteinopathy or lipidopathy? *NPJ Parkinsons Dis* **6**, 3 (2020).
77. D. Scott, S. Roy, α-Synuclein inhibits intersynaptic vesicle mobility and maintains recycling-pool homeostasis. *J. Neurosci.* **32**, 10129–10135 (2012).
78. V. M. Nemani, W. Lu, V. Berge, K. Nakamura, B. Onoa, M. K. Lee, F. A. Chaudhry, R. A. Nicoll, R. H. Edwards, Increased expression of alpha-synuclein reduces neurotransmitter release by inhibiting synaptic vesicle reclustering after endocytosis. *Neuron* **65**, 66–79 (2010).
79. Y. E. Liu, W. Pu, Y. Jiang, D. Shi, R. Dackour, Y. E. Shi, Chaperoning of estrogen receptor and induction of mammary gland proliferation by neuronal protein synuclein gamma. *Oncogene* **26**, 2115–2125 (2007).
80. M. Hirohata, K. Ono, A. Morinaga, T. Ikeda, M. Yamada, Anti-aggregation and fibril-destabilizing effects of sex hormones on alpha-synuclein fibrils in vitro. *Exp. Neurol.* **217**, 434–439 (2009).
81. M. A. Lynch, Long-term potentiation and memory. *Physiol. Rev.* **84**, 87–136 (2004).
82. B. Ji, M. Skup, Roles of palmitoylation in structural long-term synaptic plasticity. *Mol. Brain* **14**, 8 (2021).
83. M. Adlanmerini, R. Solinhac, A. Abot, A. Fabre, I. Raymond-Letron, A. L. Guihot, F. Boudou, L. Sautier, E. Vessieres, S. H. Kim, P. Liere, C. Fontaine, A. Krust, P. Chambon, J. A. Katzenellenbogen, P. Gourdy, P. W. Shaul, D. Henrion, J. F. Arnal, F. Lenfant, Mutation of the palmitoylation site of estrogen receptor α in vivo reveals tissue-specific roles for membrane versus nuclear actions. *Proc. Natl. Acad. Sci. U.S.A.* **111**, E283–E290 (2014).
84. A. Pedram, M. Razandi, J. K. Kim, F. O'Mahony, E. Y. Lee, U. Luderer, E. R. Levin, Developmental phenotype of a membrane only estrogen receptor alpha (MOER) mouse. *J. Biol. Chem.* **284**, 3488–3495 (2009).
85. K. R. Tonn Eisinger, K. M. Woolfrey, S. P. Swanson, S. A. Schnell, J. Meitzen, M. Dell'Acqua, P. G. Mermelstein, Palmitoylation of caveolin-1 is regulated by the same DHHC acyltransferases that modify steroid hormone receptors. *J. Biol. Chem.* **293**, 15901–15911 (2018).
86. J. Meitzen, K. A. Britson, K. Tuomela, P. G. Mermelstein, The expression of select genes necessary for membrane-associated estrogen receptor signaling differ by sex in adult rat hippocampus. *Steroids* **142**, 21–27 (2019).
87. G. P. H. Ho, B. Selvakumar, J. Mukai, L. D. Hester, Y. Wang, J. A. Gogos, S. H. Snyder, S-nitrosylation and S-palmitoylation reciprocally regulate synaptic targeting of PSD-95. *Neuron* **71**, 131–141 (2011).
88. J. Wan, A. F. Roth, A. O. Bailey, N. G. Davis, Palmitoylated proteins: Purification and identification. *Nat. Protoc.* **2**, 1573–1584 (2007).
89. S. Nuber, E. Petrasch-Parwez, B. Winner, J. Winkler, S. von Horsten, T. Schmidt, J. Boy, M. Kuhn, H. P. Nguyen, P. Teismann, J. B. Schulz, M. Neumann, B. J. Pichler, G. Reischl, C. Holzmann, I. Schmitt, A. Bornemann, W. Kuhn, F. Zimmermann, A. Servadio, O. Riess, Neurodegeneration and motor dysfunction in a conditional model of Parkinson's disease. *J. Neurosci.* **28**, 2471–2484 (2008).
90. S. Nuber, F. Harmuth, Z. Kohl, A. Adame, M. Trejo, K. Schonig, F. Zimmermann, C. Bauer, N. Casadei, C. Giel, C. Calaminus, B. J. Pichler, P. H. Jensen, C. P. Muller, D. Amato, J. Kornhuber, P. Teismann, H. Yamakado, R. Takahashi, J. Winkler, E. Masliah, O. Riess, A progressive dopaminergic phenotype associated with neurotoxic conversion of α-synuclein in BAC-transgenic rats. *Brain* **136**, 412–432 (2013).
91. A. J. Newman, D. Selkoe, U. Dettmer, A new method for quantitative immunoblotting of endogenous α-synuclein. *PLOS ONE* **8**, e81314 (2013).
92. B. R. Lee, T. Kamitani, Improved immunodetection of endogenous α-synuclein. *PLOS ONE* **6**, e23939 (2011).
93. J. Zhao, A. Li, M. Rajsombath, Y. Dang, D. J. Selkoe, S. Li, Soluble Aβ oligomers impair dipolar heterodendritic plasticity by activation of mGluR in the hippocampal CA1 region. *iScience* **6**, 138–150 (2018).

Acknowledgments: We thank in particular D. J. Selkoe and all members of the Nuber, Selkoe, and Dettmer laboratories for helpful discussions, W. N. Hahn (BWH) for help with histological sections, K. J. Hodgetts (BWH) for advice and help regarding ML348 chemistry, B. C. Healy (HMS) for advice regarding statistical tests, the NeuroTechnology Studio at BWH for providing Leica DMI8 and Zeiss LSM880 + Fast AiryScan Confocal Microscope access and consultation on data acquisition and data analysis, and the HMS Neuroimaging Facility (grant NS072030) for Leica SP8/STED access. **Funding:** This work was supported by National Institute of Health Grants NS109510 (to S.N.) and NS110876 (to G.P.H.H.), the Orchard Foundation, and a gift from the Women's Brain Initiative to S.N. **Author contributions:** Study concept and experimental design: S.N., S.L., and T.E.M. Biochemical αS analyses: T.D.M., T.E.M., and P.A.B. IHC/IF/PLA experiments, confocal/STED imaging, and image analysis: T.E.M. Electron microscopy scanning and image analysis: M.E. and T.E.M. Behavioral analyses: P.A.B. and S.N. Electrophysiology studies and data analysis: S.L. ABE assays and downstream experiments (WB and ELISA): G.P.H.H., T.D.M., and T.E.M. ML348 chemistry and optimization: L.N.P. Data analysis and interpretation: T.E.M., S.N., G.P.H.H., and S.L. Writing manuscript draft: T.E.M. and S.N. All coauthors provided critical inputs and edits to the manuscript. **Competing interests:** The authors declare that they have no competing interests. **Data and materials availability:** All data needed to evaluate the conclusions in the paper are present in the paper and/or the Supplementary Materials.

Submitted 9 June 2023
Accepted 18 October 2023
Published 17 November 2023
10.1126/sciadv.adj1454